國立臺灣大學工學院應用力學研究所

碩士論文

Graduate Institute of Applied Mechanics

College of Engineering

National Taiwan University

Master Thesis

奈米尺度聲子熱傳之介面效應分析

The Interface Effects on Nanoscale Phonon Heat Transfer

黃明峻

Ming-Chun Huang

指導教授：楊照彥 博士

中華民國九十七年七月

July 2008

摘要

在宏觀的尺度下，物質可視為連續體，並可由宏觀的方程式主導。當物質尺度越來越小時，特徵尺寸到達粒子間的距離，此時，連續體的假設不再適用，宏觀方程式不能準確預測物體的行為。波茲曼方程式以粒子的觀點出發，以平均的概念求得物體的行為，因此得以用來主導微觀尺度之下物體的行為。

在微觀尺度下，物質內部碰撞的次數大為減少，於是介面的反應機制更為重要。本文使用波茲曼聲子熱輻射方程式以有限差分法解一維及二維熱傳問題。探討在散射介面與鏡射介面反應機制之下，對於聲子的熱傳性質的影響。

在尺度越來越小時，兩種介面機制的熱傳係數皆減小。散射介面所得到的熱傳係數較鏡射介面為大，但是都比塊材的熱傳係數小。介面的分佈方向也影響著熱傳係數，介面的方向與熱傳方向呈垂直時，所形成的熱阻較大，熱傳係數也就越小。

Abstract

In the past decades, thermal conductivities of nanostructures have attracted considerable attention with the increased importance of nanodevices. Experimental results showed that the thermal conductivities of nanostructures are often smaller than those of their corresponding bulk material. The causes of the reduction of thermal conductivity include the micro-structural difference and the boundary and interface effects. There are two groups to model the thermal conductivities in nanostructures. One group is wave models, which assumes that phonons form superlattice bands and calculates the modified phonon dispersion using lattice dynamics. The other group is particle models, which assumes that the major reason for reduction of the thermal conduction is the scattering of phonons at interfaces. This thesis focus on the particle models in one-dimension and two-dimension nanostructures for studying the thermal conductivities.

As the size becomes smaller, the larger temperature drop at the interfaces occurs which is resulted from the ballistic transport and the effect of interface. There are many theories for treating the reaction of phonons striking onto the interface, such as acoustic mismatch model(AMM), diffuse mismatch model(DMM), and inelastic mismatch model(IDMM). The results of simulation shows that the temperature jump at the interface of acoustic model is larger than diffuse model. The thermal conductivities of

all models are decreased as the decreasing of thickness. And as the films thick, the thermal conductivity approaches the value of bulk.

TABLE OF CONTENTES

LIST OF FIGURES

LIST OF TABLES

Chapter 1

Introduction

Heat transfer is getting more important in engineering fields as the development of micordevices. We often use Fourier's law to estimate the heat transfer of thermal conduction. Fourier's law is well-predicted in macroscale, however, the prediction in the microscale region is failed. Because the assumption of continuum for Fourier's law is unreasonable in microscale region. Size effect occurs when a solid material contains defects or interfaces that are separated by a distance comparable to or smaller than the bulk mean free path of the energy carriers, which are photons, electrons, and phonons. These energy carriers are wave in nature, but at a sufficiently large size scale they can be viewed as particles. On the other hand, if the size scale of the medium is small enough to be comparable to the wavelength of the energy carriers, their transport can be affected in a different way [13][14].

The energy carriers participating in heat conduction in solids are electrons and phonons [12]. Phonons are the dominant heat carriers in non-metallic solids and semiconductors. When phonons travel through a body of semiconductor solid with no internal defects, they can experience two types of scattering, as shown in Fig.1. One type scattering is phonon-phonon scattering, in which phonon scatter after colliding with other phonons, and the other type is boundary scattering, in which phonons scatter

at the medium boundary. If the dimension of the solid medium is large, much larger than the phonon mean free path, then phonon-phonon scattering is dominant, that is, phonons will collide with other phonons many times before reaching the medium boundary. The average distance that the phonons travel between collisions with other phonons in a large medium is called the bulk phonon mean free path, which is different for each material and also change with temperature. The mean free path of phonon can be estimated form the phonon dispersion relation of the material.

If the solid medium is a thin film, in which its thickness is smaller or comparable to the phonon mean free path, then the phonon boundary scattering becomes important. In such thin films, phonons will scatter at the medium boundary before colliding with other phonons, as shown in Fig.2 .

The thermal conductivity of a non-metallic solid scales with its phonon mean free path, because the fewer times heat carriers scatter while moving across a medium, the more efficiently they can transfer their momentum and energy. The phonon mean free path reduction in thin films will also result in the decrease in their thermal conductivity. Such reduction in thermal conductivity in thin films due to phonon mean free path reduction is called the classical phonon size effect in thin films, which was observed by Casimir at low temperatures even in bulk samples.

Based on the Boltzmann transport theory, Majumdar [5] made an analogy between

heat conduction and radiation for phonons, and derived the equation of phonon radiative transfer (EPRT). The EPRT shows that in microscale regime heat transport by lattice vibrations or phonons can be analyzed as a radiative problem.

A theory which has been applied successfully at extremely low temperature is the acoustic mismatch model (AMM), which assumes all phonons interact specularly with the interface and uses the approach from continuum acoustic theory to calculate the transmission for phonons striking the interface. Another theory which has been applied at high temperature is the diffuse mismatch model (DMM), which assumes all phonon interact diffusely with the interface. The applicability of AMM and DMM is determined by the ratio λ_d/σ, where λ_d is the dominant phonon wavelength, and σ is the mean interfacial roughness. The regions of applicability of the two models can be described as that $\frac{\lambda_d}{\sigma} \gg 1$ for AMM and $\frac{\lambda_d}{\sigma} \leq 1$ for DMM [3].

The objective of the work in this thesis is to provide theoretical characterization of phonon transport in many different interface situations. Chapter 2 contains the review of literatures on the modeling of phonon transport. We introduce the governing equation for depicting the motion of particles, i.e., Boltzmann equation and the models for treating the interface phonons striking onto. Chapter 3 presents the numerical methods for simulating.Chapter 4 presents the results and the discussion.

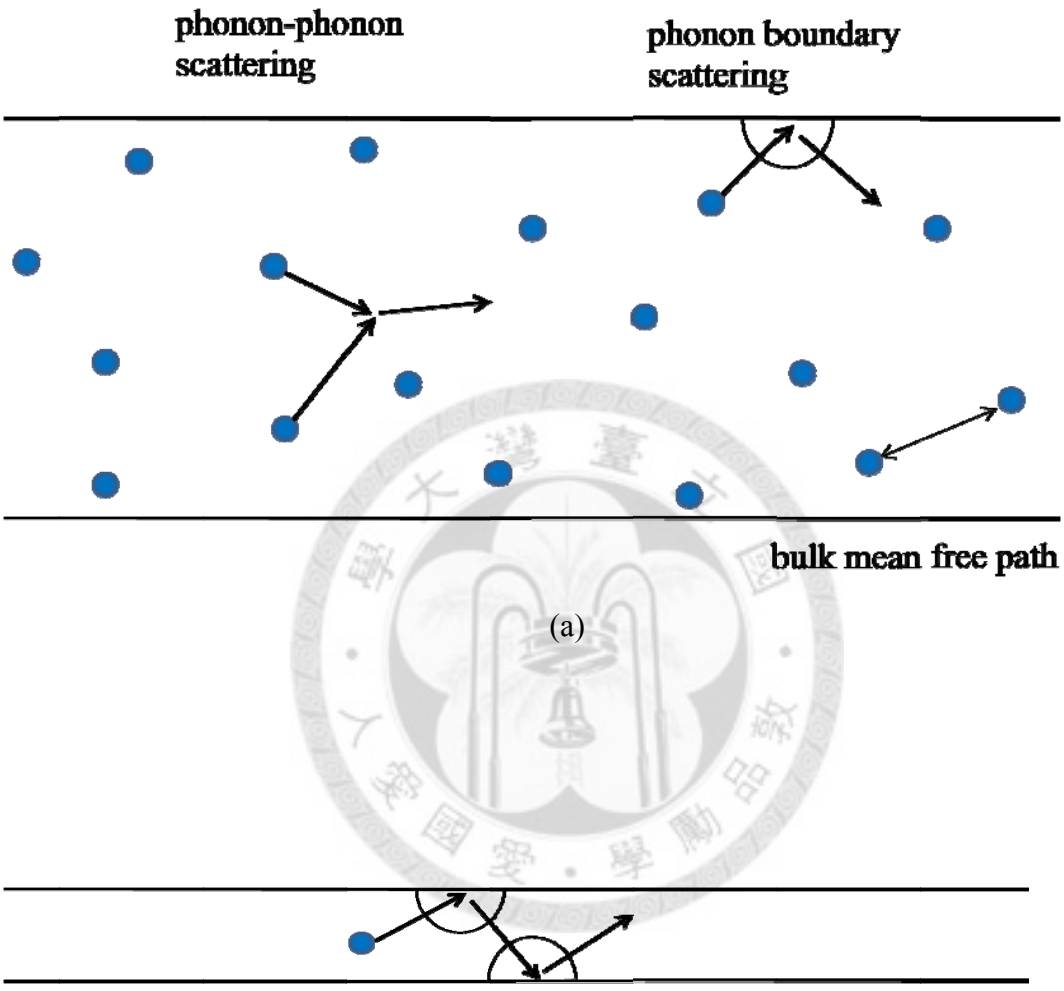

Fig. 1.1. Phonon transport in single crystal non-metallic solid: (a) bulk material (b) phonon size effect in a thin film

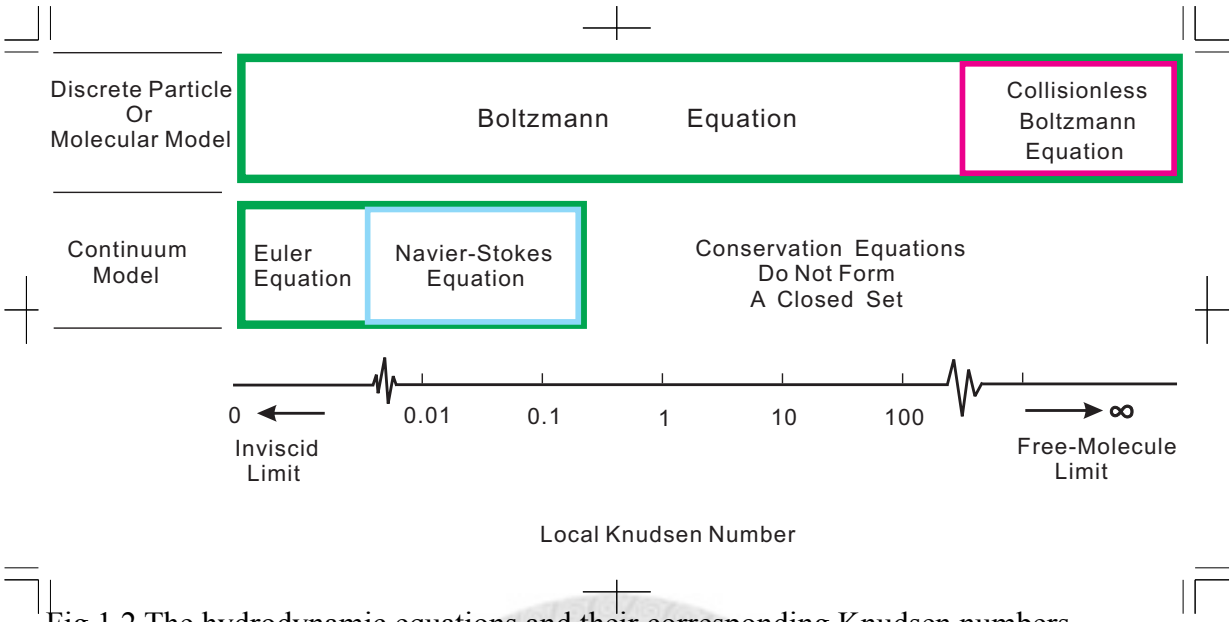

Fig 1.2 The hydrodynamic equations and their corresponding Knudsen numbers

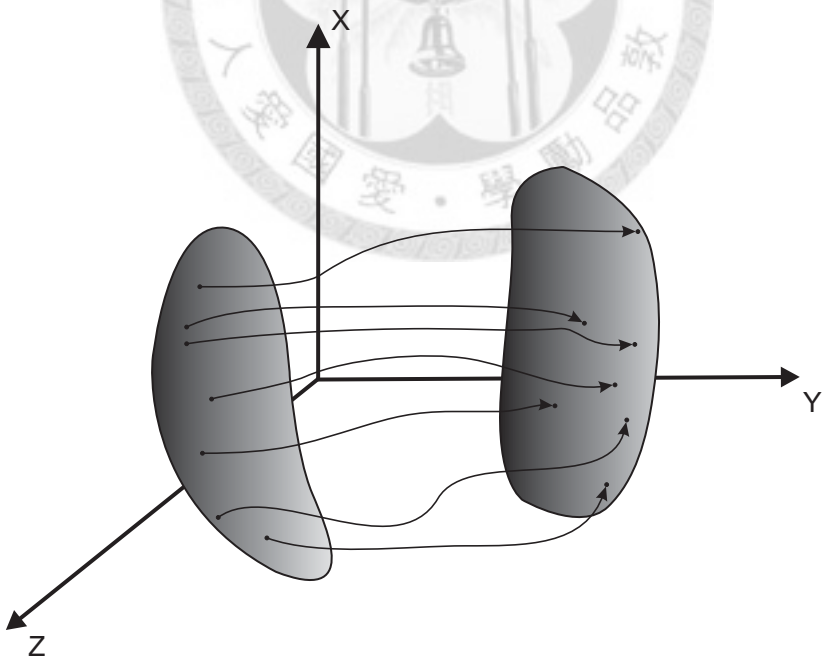

Fig 1.3 The ensemble

Chapter 2

Theory

2.1 Phonon

Consider the regular lattice of atoms in a uniform solid material. The vibrations of atoms construct packages of energy traveling through the lattice. Because of the bonds that tie the atoms together, the vibrations cannot vibrate arbitrary. The vibrations take the form of collective modes which propagate through the material. The propagation lattice vibration is considered to be sound of waves, and their propagation speed is the speed of sound in the material. The vibrational energies of molecules are quantized and treated as quantum harmonic oscillators. Quantum harmonic oscillators have equally spaced energy levels with the separation, $\varepsilon = \hbar\omega$, therefore, the oscillators can accept or lose energy only in discrete units of energy.

The quantum of energy is called a phonon. Phonon is analogy with the photon of the electromagnetic waves. The equilibrium distribution obeys Bose-Einstein distribution.

$$f(T) = \frac{1}{e^{\varepsilon-\mu/kT} - 1} \tag{2-1}$$

In the Deybe model, the velocity of sound is constant for each polarization, the dispersion relation is [4]

$$\omega = vk \tag{2-2}$$

Here, ω is the angular frequency, v is the velocity, and k is the wave vector. The density of state is

$$D(\omega) = \frac{\omega^2 V}{2\pi^2 v^3} \tag{2-3}$$

The thermal energy is given by

$$U = \int D(\omega) f(T) \hbar\omega d\omega = \int_0^{W_D} \frac{\omega^2 V}{2\pi^2 v^3} \cdot \frac{\hbar\omega}{e^{\varepsilon-\mu/kT} - 1} d\omega \tag{2-4}$$

The heat flux is

$$U = \int v D(\omega) f(T) \hbar\omega d\omega = \int_0^{W_D} \frac{\omega^2 V}{2\pi^2 v^2} \cdot \frac{\hbar\omega}{e^{\varepsilon-\mu/kT} - 1} d\omega \tag{2-5}$$

	electron	phonon	photon
generation	Ionazation,excitation	Lattice vibration	Atomic, molecule transition
statistics	Fermion	boson	boson
velocity	$\sim 10^{6}$ m/s	$\sim 10^{3}$ m/s	$\sim 10^{8}$ m/s

Table 1.1 The properties of heat carriers

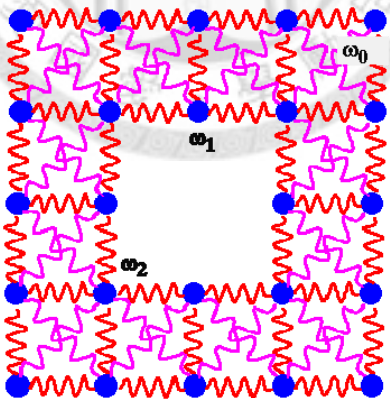

Fig. 2.1 The model for lattice vibration

2.2 Boltzmann Transport Equation

Boltzmann transport equation (BTE) is a general fundamental equation for treating energy transport problem[2],

$$\frac{\partial f}{\partial t} + \boldsymbol{v} \cdot \nabla_{\boldsymbol{r}} f + \boldsymbol{a} \cdot \nabla_{\boldsymbol{v}} f = \left(\frac{\partial f}{\partial t}\right)_{\text{collision}} \tag{2-6}$$

where f is the statistical distribution function for an ensemble of particles, $\boldsymbol{v}$ the particle vector, $\boldsymbol{a}$ the particle acceleration which external force applied to the particle. Equation (10) states that f varies with time t, particle position vector $\boldsymbol{r}$, and particle velocity $\boldsymbol{v}$. The left hand side of Eq. (10) is called drift term, which represents the collective drift of the phonon ensemble away from the equilibrium state, and the right hand side of the equation is called collision term, representing the collision mechanisms that restores the phonon ensemble to equilibrium.

The third term on the left hand side of Eq. (10) is nonzero only in the presence of external applied force on the particles. For the phonon transport, the force does not exists. Phonon heat conduction is only due to the temperature difference from a higher population density to a lower population density.

Since BTE describes energy as being carried by discrete heat carriers, it can be used to treat microscale or nanoscale energy transport, in which the mean free path is comparable or larger than the characteristic size of the host medium. At the other extreme , BTE can also be reduced to the classical macroscale energy transport

equations, such as Fourier's Law of heat conduction, Fick's Law of diffusion, Euler's equation and Naiver-Stokes equation of fluid dynamics. Although it is so powerful, Boltzmann transport equation is difficult to solve, because it has many variables : position, momentum, and time.

2.3 Equation of Phonon Radiative Transport

Heat transport in dielectric crystalline materials is predominantly by lattice vibration. These vibrations travel in the solid as waves. The energy of these waves is quantized as particles. Using an analogy to photons, an intensity of phonon can be defined as[5][8]

$$I_\omega(\theta,\phi,r,t) = \frac{1}{4\pi}\sum_p \mathrm{v}(\theta,\phi) f_\omega(\mathrm{r},t)\hbar\omega D(\omega) \qquad (2\text{-}7)$$

Here $\boldsymbol{v}$ is the group velocity of phonons in the direction of (θ,ϕ) within a unit solid angle, $\hbar\omega$ is the energy of a package of phonons and $D(\omega)$ is the density of state per unit volume. This makes the intensity the flux of energy per unit time, per unit area, per unit solid angle in the direction of phonon propagation and per unit frequency interval around ω. Mulitiplying Eq.(10), the Boltzmann equation can be transformed to

$$\frac{1}{v}\frac{\partial I_\omega}{\partial t} + \boldsymbol{s}\cdot\nabla_{\boldsymbol{r}} I_\omega = \frac{I_\omega^e(T(x)) - I_\omega}{v\tau(\omega,T)} \qquad (2\text{-}8)$$

Where $\boldsymbol{s}$ is the unit direction of the propagation the group velocity v and I_ω^e is the equilibrium intensity corresponding to a black body intensity at temperatures below the

Debye temperature. For phonons, the velocity of propagation maintains constant, therefore, the acceleration term is zero. The Eq.(12) is called the equation of phonon radiative transport. Once the intensity is found by solving the EPRT, the heat flux can be determined as

$$q(x) = \int_{\Omega=4\pi} \int_0^{\omega_D} \mu_x I_\omega(x,\omega,\Omega) d\omega d\Omega \tag{2-9}$$

where μ_x is the projection value of intensity onto x-direction. For steady state, the phonon intensity is in equilibrium when there is no source energy, that is $\nabla \bullet \boldsymbol{q} = 0$. This is the first law of thermodynamics. The expression is given by

Integrating the one-dimensional EPRT over $-1 < \mu < 1$ and over all the frequencies, the following equation is derived,

$$\begin{aligned} &\frac{\partial I_\omega}{\partial t} = 0 \\ &\frac{dq}{dx} = \frac{d}{dx} \int_{\Omega=4\pi} \int_0^{\omega_D} \mu_x I_\omega(x,\omega,\Omega) d\omega d\Omega \\ &\quad = 2\int_0^{\omega_D} \frac{I_\omega^e}{v\tau(\omega,T)} d\omega - \int_0^{\omega_D} \frac{d\omega}{v\tau(\omega,T)} \left(\int_{-1}^{1} I_\omega d\mu\right) \\ &\quad = 0 \end{aligned} \tag{2-10}$$

Under phonon radiative equilibrium, $dq/dx = 0$, and therefore the two terms of EPRT on the right side become equal. To obtain an easy approximate solution, we could assume that a stringent condition of equilibrium at every frequency to get

$$I_\omega^e = \frac{1}{2}\int_{-1}^{1} I_\omega d\mu \tag{2-11}$$

The assumption is valid only when the medium is gray, the relaxation time is

independent of the frequency. Integrate the Eq.(222) over all frequencies and the temperature is much lower than the Debye temperature, then

$$\frac{\sigma T^4}{\pi} = \frac{1}{2}\int_0^{\omega_D}(\int_{-1}^{1} I_\omega d\mu) d\omega \qquad (2\text{-}12)$$

Therefore, the temperature could be obtained at any position via the intensity.

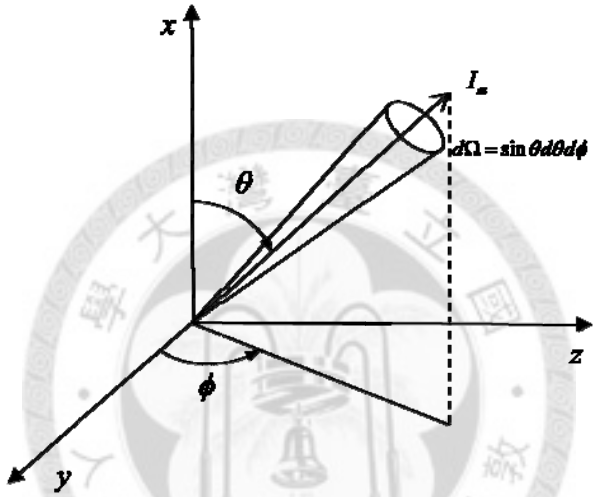

Fig 2.2 The space in solid angle

2.4 Relaxation Time Approximation

Because of the complexity of the collision term, it is common to use the Bhatnagar Gross Krook (BGK) approximation.

$$(\frac{\partial f}{\partial t})_{collision} = \frac{f^{(e)} - f}{\tau} \qquad (2\text{-}13)$$

where $f^{(e)}$ is the equilibrium distribution, and τ is the relaxation time which means the interval time between two collisions.

Fourier's Law

Fourier's law states that the time rate of heat transfer per unit area through a material is proportional to the negative gradient temperature, and the expression is

$$\dot{q} = -k\nabla T \tag{2-14}$$

The Fourier's law can be obtained from the Boltzmann equation by two assumptions. One assumption is that the characteristic length is much larger than the mean free path,

2.5 Relaxation Time

Phonons traveling in a solid may be scattered by a variety of mechanisms, including impurities, isotopes, defects, material boundaries as well as other carriers such as electrons or other phonons. Scattering interaction may be characterized as elastic, in which the energy of phonon remains unchanged as a result of the scattering event; or as inelastic, in which the energy are changed during the event. Scattering due to dislocations, impurities, and isotopes are elastic, the events only change the direction of traveling. Two main types of inelastic scattering processes are important for thermal transport, normal and Umklapp processes. These processes are called intrinsic processes. Three phonon processes can involve two phonons combining to form one, or conversely, one phonon can splitting into two. Three phonon processes are governed by energy and momentum conservation rules, the expressions are given by

$$\begin{aligned} &\omega + \omega' \Leftrightarrow \omega'' && N \text{ and } U \text{ processes} \\ &K + K' \Leftrightarrow K'' && N \text{ process} \\ &K + K' \Leftrightarrow K'' + G && U \text{ processes} \end{aligned} \tag{2-15}$$

Both N and U processes satisfy energy conservation, N processes satisfy the momentum conservation, but U processes do not satisfy momentum energy conservation. The U processes do not contribute the thermal equilibrium because of the momentum conservation. The U processes would occur the thermal transport because the momentum do not conserve. The relaxation time for U processes is given by

$$\tau_U = A\frac{T}{T_D}\exp(T_D / \gamma T) \tag{2-16}$$

where A and γ are the material properties, is T_D is the Debye temperature.

The impurity scattering is an important role for the mean free path. The relaxation time due to the impurity is given by

$$\tau_i = \frac{1}{\alpha\varphi\psi v} \tag{2-17}$$

here φ is scattering area, ψ is the impurity density, and v is the phonon velocity. The scattering area can be expressed as

$$\varphi = \pi R^2 (\frac{\chi^4}{\chi^4 + 1}) \tag{2-18}$$

where R is the radius of lattice impurity, and χ is the dimension parameter.

The effective relaxation time can be estimated using Mattheissen's Rule

$$\frac{1}{\tau} = \frac{1}{\tau_U} + \frac{1}{\tau_i} \tag{2-19}$$

2.6 Gray Model Approximation

A rigorous phonon transport simulation should incorporate with the frequency dependence of the phonon relaxation time and group velocity, and the interactions among the dispersive phonons of different frequencies should take into account. It needs to solve the phonon BTE for many different frquencies. However, previous works show that an average MFP is a good approximation for thermal conductivity.

Often the phonon MFP Λ is estimate from the kinetic theory

$$k = \frac{1}{3} C v \Lambda$$

where C is the volumetric specific heat, k is the thermal conductivity, and v is the group velocity. This method neglects the fact that the phonons are highly dispersive.

1.7 Boundary Conditions

The action of the phonon intensity striking into the boundary is more important in microscale, since the boundary resistance plays an important part compared to the total thermal resistance[11].

1.7.1 Black Body Boundary Condition

Assume the emitted intensity is the intensity at the equilibrium state, which is related with the equilibrium temperature.

2.7.2 Equlibrium Temperature Boundary Condition

Assume the sum of all the intensities is the same as the sum of intensity at equilibrium temperature.

$$\int_{4\pi} I^e(\boldsymbol{r},\boldsymbol{s})d\Omega = \int_{\boldsymbol{s}\cdot\boldsymbol{n}>0} I(\boldsymbol{r}_{bc},\boldsymbol{s})d\Omega + \int_{\boldsymbol{s}\cdot\boldsymbol{n}<0} I(\boldsymbol{r},\boldsymbol{s})d\Omega \tag{2-20}$$

Assume the intensity in any direction is the same. Therefore, the emitted intensity is

$$I(\boldsymbol{r}_{bc},\boldsymbol{s}) = \frac{4\pi I^e - \int_{\boldsymbol{s}\cdot\boldsymbol{n}<0} I(\boldsymbol{r},\boldsymbol{s})d\Omega}{\int_{\boldsymbol{s}\cdot\boldsymbol{n}>0} d\Omega} \tag{2-21}$$

2.8 Interface Conditions

There are two extreme limited events for the phonons striking into the interface. In low temperature circumstance, the phonon goes to the specular limit; in high temperature circumstance, the phonon goes to the diffuse limit. But in room temperature, the phonons scatter at the interface not only in specularity, but also in diffusely. The interface would scatter phonons partially specularly and partially diffusely, the boundary conditions are combined by two parts with a ratio, specularity parameter p, therefore, the phonon intensity of both sides at interface are

$$I_2^+(0,\mu_2) = p[R_{s21}(\mu_2)I_2^-(0,-\mu_2) + t_{s12}(\mu_1)I_1^+(\xi_1,\mu_1) + (1-p)[2R_{d21}\int_{2\pi} I_2^-(0,-\mu_2)\mu_2 d\mu_2 +$$

$$2T_{d12}\int_{2\pi} I_1^+(\xi_1,\mu_1)\mu_1 d\mu_1]$$

$$I_1^-(\xi_1,-\mu_2) = p[R_{s12}(\mu_1)I_1^+(\xi_1,-\mu_1) + t_{s21}(\mu_2)I_2^-(0,-\mu_2) + (1-p)[2R_{d12}\int_{2\pi} I_1^+(\xi_1,\mu_1)\mu_1 d\mu_1 +$$

$$2T_{d21}\int_{2\pi} I_2^-(0,-\mu_2)\mu_2 d\mu_2] \qquad \text{(2-22)}$$

where R_{sij} and T_{sij} are the speculary reflectivity and transmissivity for phonons incident from layer i to layer j.

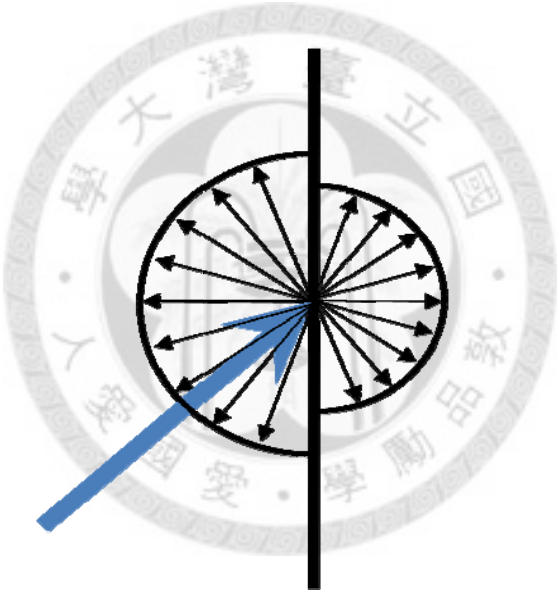

(a)

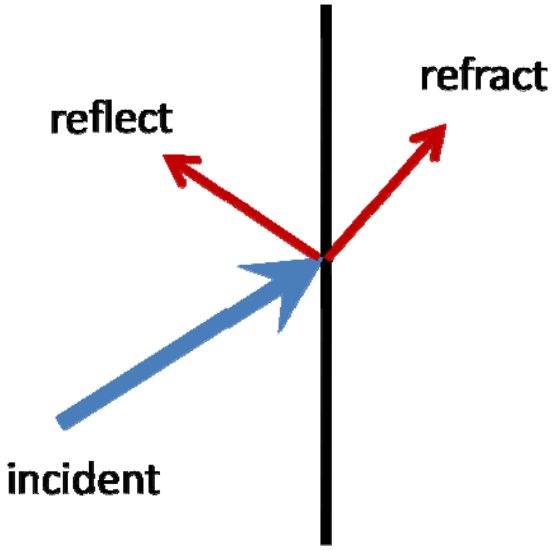

(b)

Fig.2.3 The mechanism of phonon striking onto the interface. (a) diffuse scattering: the reaction is isotropic. (b) specular scattering: the reaction is mirror-like

2.8.1 Elastic Acoustic Mismatch Model

The AMM model is based on the premise that all of the phonons are specular in nature [6]. From the AMM theory the transmission coefficient is depend upon the mode j of the incident phonon, that is whether it is vibrating longitudinally, parallel transversely, or perpendicular transversely. As the transmission coefficient represents the ratio of the transmitted energy to the incident energy, the phenomenon of mode conversion, which occurs at the interface of the two materials, will also affect the value of transmission coefficient. In the interest of evaluating the feasibility of our proposed model mode conversion is not consideration. The assumption is made that the incident

waves are traveling at the same speed in all directions. The value of the speed in material 1 is taken as

$$c_1 = (\sum_j c_{1,j}^{-2})^{-0.5} \tag{2-23}$$

Here, j is the mode of vibration. The transmission coefficient is given by

$$T_{12} = \frac{4\frac{\rho_2 c_2}{\rho_1 c_1}\cdot\frac{\cos\theta_2}{\cos\theta_1}}{(\frac{\rho_2 c_2}{\rho_1 c_1}+\frac{\cos\theta_2}{\cos\theta_1})^2} \tag{2-24}$$

where ρ_1 and ρ_2 are the density of the media, θ_1 and θ_2 are the angle of incidence of the phonon measured from the normal to the surface. The derivation is attached in Appendix . As the transmission coefficient in the AMM case is dependent upon the angle of incidence, an integrated coefficient Γ is often used, and is given by

$$\Gamma_{12} = \int_0^{\pi/2} T_{12}\sin\theta\cos\theta d\theta \tag{2-25}$$

The upper limit of the integral actually is dependent upon the maximum possible value which is determined by the two materials. This critical angle is given by Snell's law

$$\theta_c = sin^{-1}(\frac{v_1}{v_2}) \tag{2-26}$$

The total reflection will occurs, when the angle of incident is lager than the critical angle. The reflectivity should become one, and transmissivity is zero.

$$R_{s12}(\mu_1) = 1 \qquad \text{and} \qquad T_{s12}(\mu_1) = 0 \tag{2-27}$$

The refraction angle is determined by Snell's law

$$\frac{\sin\theta_1}{v_1} = \frac{\sin\theta_2}{v_2} \tag{2-28}$$

Using Eqs.(2-23-2-28), the analytical expression for heat flux is determined as

$$q = \frac{k^4\pi^2}{60\hbar^3}[\frac{\Gamma_{12}}{c_1^2}(T_1^4 - T_2^4)] \tag{2-29}$$

The AMM limit for interface resistance R as $\Delta T \to 0$ is given by [10]

$$R = [\frac{k^4\pi^2}{15\hbar^3}(\frac{\Gamma_{12}}{c_1^2})]^{-1}T_2^{-3} \tag{2-30}$$

The acoustic mismatch model would applicable when the roughness of interface is small, in which situation the wavelength is larger than the surface roughness. [Phelan]

2.8.2 Inelastic Acoustic Mismatch Model

Chen (1998) proposed the inelastic acoustic mismatch model [1]. The model assumes that the scattering interaction at interface is inelastic. The relation of the reflection angle and transmission angle is

$$\frac{\mu_1}{\mu_2} = (\frac{C_2 v_2}{C_1 v_1})^{1/2} \tag{2-31}$$

In the low-temperature limit, the relation would go back to the elastic model.

2.8.3 Elastic Diffuse Mismatch Model

In the diffuse mismatch model the assumption of complete specularity is replaced with the opposite extreme [9]: all the phonons are diffusely scattered at the interface. In the diffuse mismatch model, acoustic correlations at interfaces are assumed to be

completely destroyed by diffuse scattering, so that the only determinants of the transmission probability are densities of phonon states and the principle of detailed balance.

The effect on the thermal boundary resistance of diffuse scattering at the interface can be qualitatively determined with the following arguments. Assume that scattering destroys the correlation between the wave vectors of incoming and outgoing phonons; the scattered phonons forget where it came from. The probability of scattering into a given side is proportional to the density of phonon states and is also restricted by the principle of detailed balance. A phonon with energy $\hbar\omega_i$, wave vector $\boldsymbol{k_i}$, and mode j_i is diffusely scattered if the resulting phonon's wave vector $\boldsymbol{k_f}$ and mode j_i are completely independent of $\boldsymbol{k_i}$ and j_i. After a diffuse scattering event, a phonon loses the memory of where it came from and what mode it was.

$$T_{di,j}\left(\omega,\boldsymbol{k}\right)=T_{di,j}(\omega) \tag{2-32}$$

Since a phonon forgets where it came from, the probability of reflection from one side must equal the probability of transmission from the other side. The expression is given by

$$T_{d12}(\omega)=1-T_{d21}(\omega) \tag{2-33}$$

We also assume that the scattering events are elastic.

$$\hbar\omega_i=\hbar\omega_j \tag{2-34}$$

The number of phonons of energy $\hbar\omega$ per unit area per unit time leaving side i is

$$\sum_j \int_0^{2\pi} \int_0^{\pi/2} v_{i,j} f_{i,j}(\omega, \mathrm{T}) \mathrm{T}_i(\omega) \cos\theta d\theta d\phi \qquad (2\text{-}35)$$

Here, $f_{i,j}(\omega, \mathrm{T})$ is the density of phonons with energy $\hbar\omega_i$ on side i with mode j at temperature T. Because the transmission probabilities are independent of incident angle, the angular integrals is given by

$$\frac{1}{4}[\sum_j v_{i,j} f_{i,j}(\omega, T)]\alpha_i(\omega) \qquad (2\text{-}36)$$

From the detail balance, this must equal the number of phonons of energy $\hbar\omega$ leaving side $3-i$ per unit area per unit time:

$$\sum_j v_{i,j} f_{i,j}(\omega, T)\alpha_i(\omega) = \sum_j v_{3-i,j} f_{3-i,j}(\omega, T)[1-\alpha_i(\omega)] \qquad (2\text{-}37)$$

From this the transmission probabilities can be determined, which is given by

$$T_i(\omega) = \frac{\sum_j v_{3-i,j} f_{3-i,j}(\omega, T)}{\sum_{i,j} v_{i,j} f_{i,j}(\omega, T)} \qquad (2\text{-}38)$$

We shall make the Debye approximation for the phonon velocities and phonon densities of states. The transmission coefficients can be written as

$$T_i(\omega) = \frac{\sum_j v_{3-i,j}^{-2}}{\sum_{i,j} v_{3-i,j}^{-2}} \qquad (2\text{-}39)$$

2.8.3 Inelastic Diffuse Mismatch Model

Assume that the scattering at the interface can be inelastic, so that, the phonons of all frequencies can transmit through the interface, and phonons in one layer with frequency

higher than the maximum frequency of phonons in the adjacent layers can transmit into adjacent layers by splitting into two or more phonons through anharmonic interatomic interactions. In the diffuse scattering model, these inelastic-scattering processes redistribute phonons isotropically in all directions [3].

Chap 3

Numerical Method

3.1 Nondimensional variables

For solving the equations, transform the variables into nondimensional variables. The reference length is set as the thickness of film, the reference group velocity as the group velocity of left material and the reference specific heat as the specific heat of the left material. The reference intensity is product of specific heat, group velocity and temperature of the right boundary, and divided into 4π. The time reference would be the value that the reference length divided into reference velocity. The expressions are present as following

$$\begin{aligned} x_0 &= L_1 & I_0 &= \frac{c_0 v_0 T_0}{4\pi} \\ v_0 &= v_1 & & \\ c_0 &= c_1 & \Delta I &= \frac{c_0 v_0 \Delta T}{4\pi} \\ t_0 &= \frac{x_0}{v_0} & \Delta T &= T_H - T_o \end{aligned} \tag{3-1}$$

Therefore, nondimensioal variables are the dimensional variables divided into reference parameters, respectively. The intensity is determined by its corresponding temperature. The expressions are

$$\begin{aligned} \hat{x} &= \frac{x}{x_0} & \hat{v}_i &= \frac{v_i}{v_0} & \hat{\tau}_i &= \frac{\tau_i}{t_0} \\ \hat{t} &= \frac{t}{t_0} & \hat{c}_i &= \frac{c_i}{c_0} & \hat{T} &= \frac{T - T_0}{T_H - T_0} \end{aligned} \tag{3-2}$$

$$I_i = \frac{c_i \nu_i T_i}{4\pi} = \frac{\hat{c}_i c_0 \hat{\nu}_i c_0 \left(\hat{T}_i \Delta T + T_0\right)}{4\pi} = \hat{I}_i \Delta I + \hat{c}_i \hat{\nu}_i I_0 \qquad (3\text{-}3)$$

Substitute the nondimensional variables into the EPRT, the equation becomes

$$\frac{1}{\hat{\nu}_i}\frac{\partial \hat{I}_i}{\partial \hat{t}} + \mu \frac{\partial \hat{I}_i}{\partial \hat{x}} + \eta \frac{\partial \hat{I}_i}{\partial \hat{y}} + \xi \frac{\partial \hat{I}_i}{\partial \hat{z}} = \frac{\hat{I}_i^e - \hat{I}_i}{\hat{\nu}_i \hat{\tau}_i} \qquad (3\text{-}4)$$

Here, μ, η *and* ζ are the direction, that is, $\mu = \cos\theta, \eta = \sin\theta\cos\theta$ *and* $\zeta = \sin\theta\sin\phi$.

3.2 Discrete Ordinate Method

The EPRT is an integral-differential equation. The integral part is resulted from calculating the phonon intensity in solid angle. The integral value is obtained by summing the discrete weighted value in real space. The expression is [7]

$$\int_{4\pi} f(\hat{s}) d\Omega \approx \sum_{n=1}^{N} w_n f(\hat{s}_n) \qquad (3\text{-}5)$$

Here w_n is the weighting value in $\hat{s}_n$ direction. The weighting values are obtained by the Gauss-Legendre quadreture foumula. In three-dimension, the solid angle is approximated by 2 sets of summation, since there are two degree of freedom in solid angle space. The expression is written as

$$\begin{aligned} \int_{4\pi} f(\hat{s}) d\Omega &= \int_0^{2\pi}\int_{-1}^{1} f(\hat{s}) d\mu d\phi \\ &= \sum_{i=1}^{N}\sum_{j=1}^{M} w_{\mu,i} w_{\phi,j} f(\mu_i, \phi_j) \end{aligned} \qquad (3\text{-}6)$$

3.3 Upwind Scheme

The EPRT contains partial differentials in real space and time space. The partial differential in real space is simulated by upwind scheme. If the velocity is positive, the differential is simulated by backward scheme. Similarly, if the velocity is negative, the differential is simulated by forward scheme. The schemes met the physical meaning, which is the way that the wave travels. For example, the differential equation is

$$\frac{\partial u(x,t)}{\partial t} + v\frac{\partial u(x,t)}{\partial x} = 0 \tag{3-7}$$

Using the upwind scheme, the differential term is approximated in

$$\frac{\partial u_i}{\partial t} + v^{+}\frac{u_i - u_{i-1}}{\triangle x} + v^{-}\frac{u_{i+1} - u_i}{\triangle x} = 0 \tag{3-8}$$

where $v^{+} = \frac{v+|v|}{2}$ *and* $v^{-} = \frac{v-|v|}{2}$, the choice of grid points decided by the traveling direction of the wave, it matches the physical meaning, therefore, the scheme is stable.

The EPRT approximated by the upwind scheme for the differential term of space can be expressed as

$$\frac{1}{v}\frac{\partial I_{i,j,n,m}}{\partial t} + \mu_n^{+}\frac{I_{i,j,n,m} - I_{i-1,j,n,m}}{\Delta x} + \mu_n^{-}\frac{I_{i+1,j,n,m} - I_{i,j,n,m}}{\Delta x}\eta_m^{+}\frac{I_{i,j,n,m} - I_{i-1,j,n,m}}{\Delta y} + \eta_m^{-}\frac{I_{i+1,j,n,m} - I_{i,j,n,m}}{\Delta y}$$
$$= \frac{\frac{1}{4\pi}\sum_{n'}^{N}\sum_{m'}^{M} w_{n'}w_{m'}I_{i,j,n',m'} - I_{i,j,n,m}}{v\tau} \tag{3-9}$$

where N and M are the number of gird points, $w_n^{'}$ and $w_m^{'}$ are the weighting values decided by Gauss-Legendre quadrature.

The heat flux is determined by

$$\hat{q}_{i,j} = \sum_{n=1}^{N_n} \sum_{m=1}^{N_m} w_n w_m \mu_n \hat{I}_{i,j,n,m} \tag{3-10}$$

The calculating of the effective thermal conductivity is given by

$$k = q \frac{|\Delta x|}{|\Delta T|} \tag{3-11}$$

where Δx is the length of thickness, and ΔT is the temperature difference between two boundaries.

3.4 Steady State Condition

The criteria for determining the state in steady state is that the difference of intensities in two steps is less than 10^{-9}. If the intensities satisfy the criteria at every position, we shall consider the situation as steady state. The expression is given by

$$\left| \frac{I_{i,j,n,m}^{k+1} - I_{i,j,n,m}^{k}}{I_0} \right| < 10^{-9} \tag{3-12}$$

here k is the time step.

Chapter 4
Results and Discussion

Sample calculations carried out for GaAs/AlAs, as shown in Fig. 4.1. The properties of material are listed in Table 4.1. The boundary conditions are set as 300.1K at left and 300K at right with blackbody radiation boundary. The slight temperature difference makes the material properties to maintain almost the same through the whole medium and gets rid of the temperature-dependence of material properties, such as the specific heat, mass density, and the mean free path. So that, we can focus on the effects of interface.

4.1 The transmission and reflection intensities

In the case of specular interface, the relation of the refraction angle and incident angle is shown is Fig.4-2. The transmission reflection coefficients are shown in Fig. 4.3~4.4. Because of the velocity of GaAs is smaller than AlAs, the defraction angle will larger than the incident angle, and it will occur total reflection as the incident angle beyond the critical angle. The toally reflection will reduce the ability of phonon transport.

In the case of diffuse case, the transmission is independent of the incident angle. The transmission and reflection coefficients are always the same, and are around 0.5.

4.2 The temperature distribution

Figs. 4.9, 4.11, 4.13 and 4.15 show the distribution of the dimensionless equilibrium temperature profile for several thickness based on the elastic acoustic mismatch model and elastic diffuse mismatch model, respectively. The temperature distribution tends to be flat with the smaller of thickness. Till the thickness shrinks to 10nm, the temperature inside the substrate is almost uniform because no scattering inside the substrate is considered. The temperature jump at the film substrate interface is the smallest for diffuse interface. The temperature drop at the boundaries occurs because of the assumption of the black emitting surface. The inelastic model predicts a slightly smaller temperature drop at the interface because of a lager phonon transmissivity predicted under the model. As the thickness is 1000nm, the temperature jumps at interface are 0.015 for p=0.0 and 0.137 for p=0.5 and 0.219 for p=1.0, in which p=0.0 means totally diffuse interface, p=1.0 means totally specular interface, and p=0.5 means the ratio to diffuse and specular interface. As the thickness is 200nm, the temperature jumps at interface are 0.115 for p=0.0 and 0.187 for p=0.5 and 0.251 for p=1.0. With the decrease of the thickness, the temperature drops at the boundary and interface are getting larger, the phenomenon is shown in Fig. 4.17~4.18. Fig.4.19 depicts the temperature jumps at interface as a function of thickness.

Compare with Fourier's law, The temperature distribution solved by Fourier's law

is shown in Fig. 4.7. The boundaries of both sides are continued, and there is no drop at the interface.

4.3 The heat flux

Figs.4.8, 4.10, 4.12, 4.14, 4.16 shows the distribution of heat flux for 10nm, 100nm, and 1000nm. The heat flux at each part of material is the same at steady state, in which the steady state is in the situation that for every point the temperature difference is less than 10^{-7} in nondimensional temperature. This is obeyed concept of the conservation of energy. But, at the interface, it occurs heat flux drop for $p \neq 0$ since the velocity of the left material is smaller than that of the right material. The angle of the intensity after encountering the interface would become larger, therefore, the intensity should change its the direction of traveling from x component to y component.

4.4 The Effective thermal conductivity

Fig. 4. shows the simulated effective thermal conductivity as a function of the film thickness. The effective thermal conductivity is defined as

$$k_{eff} = \frac{q}{\Delta T} L$$

where q is the heat flux, ΔT is the temperature difference between the two reservoirs , and L is the thickness. Because of the interface scattering, the thermal conductivity is

lowered when the thickness is comparable to the mean free path. When the film becomes thicker, the thermal conductivity approaches the bulk value as expected. The thermal conductivity for AMM is smaller than the DMM, because the intensity will refract at the interface and totally reflect at the incident angle larger than

$$\theta_c = \sin^{-1}\frac{v_1}{v_2} = 59.4°$$

In the situation of the total refection, the forward intensity turns back. This mechanism minimizes the ability of heat transfer, therefore, the thermal conductivity of AMM is lower than that of DMM.

4.5 Two dimensional inplane Sample

Fig.4.21~4.36 show the two dimensional inplane samples with their corresponding temperature distributions and heat flux distributions. The samples are divided into several parts to establish the sequential number of interfaces. Although the divided length of those part are not always the same, the area of both material are the same. The effective thermal conductivities in Fourier's law shall be the same. The objective of these samples is to test the effect of interface paralleled to the direction of the heat flux.

The temperature distributions occur slight shift at the interfaces. The heat flux decreases slightly in the layer of AlAs. Fig.4.37 show the heat flux in x-direction as a function of the number of layers, the heat flux almost maintains their value. It shows

that the effect of interface only occurs for the interface perpendicular to the direction of heat flux.

4.6 Conclusion

This work applies the energy transport model that was developed for the steady state heat transfer across thin films for the case of transient heat conduction in double layer thin film structures in two different type of interface condition. The integral-differential equations are solved numerically, and the results for the events of the films thickness and profiles on temperature, heat flux, and thermal conductivity are presented. The temperature jumps that occur at the boundaries due to the phonon scattering lead to an increase in the overall thermal resistance as compared with the classical conduction case. By increasing the thickness of the films , the ballistic mechanism of heat transfer disappears, and the effective thermal conductivity of structure approaches that of the bulk value. The effective thermal conductivity depends on the thickness of the layers and increases by increasing the thickness. The acoustic mismatch model has smaller thermal conductivity than diffuse mismatch.

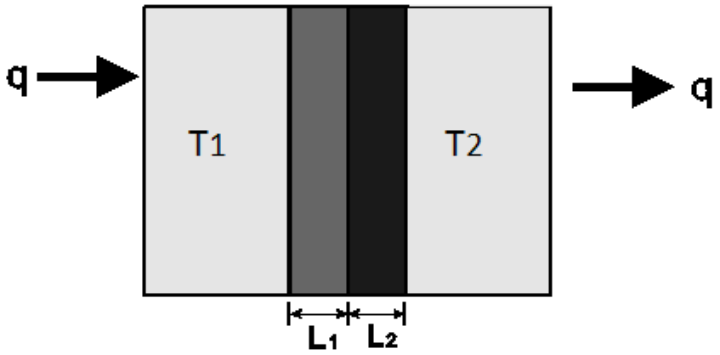

Fig. 4.1 The model for one-dimensional sample.The material for L1 is GaAs, and the material for L2 is AlAs.

Material	Specific heat $C\ (10^{6}\ J/m^{3}/K)$	Group velocity υ (m/sec.)	Mean free path Λ (Å)	Mass density ρ (kg/m^{3})
GaAs	1.71	3700	208	5318
AlAs	1.58	4430	377	3830

Table 4.1 The table of material properties

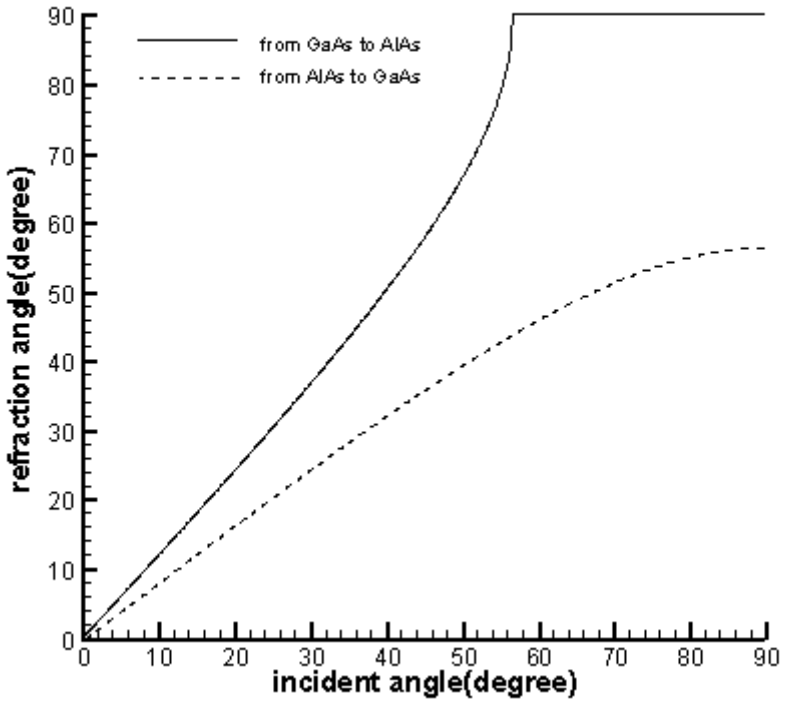

Fig. 4.2 The relation of refraction angles and incident angles for AMM.

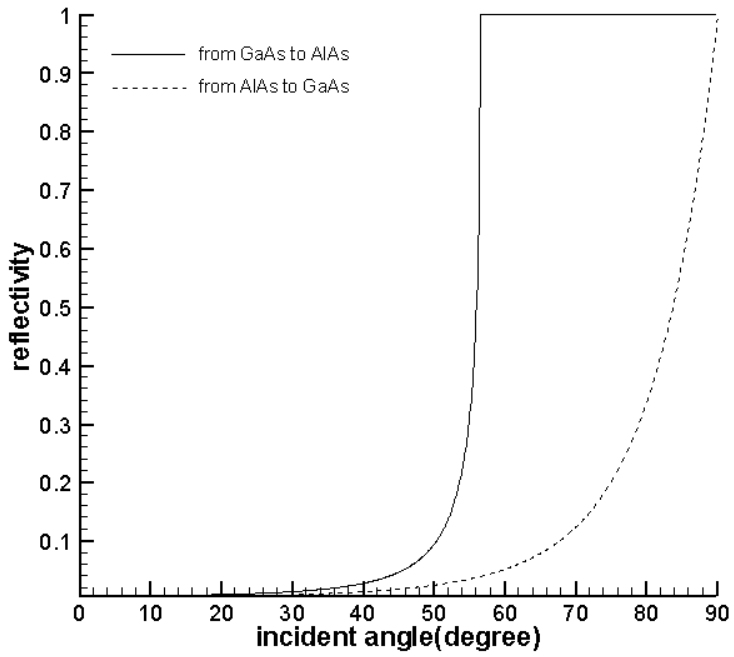

Fig. 4.3 The relation of reflection coefficient and incident angles for AMM.

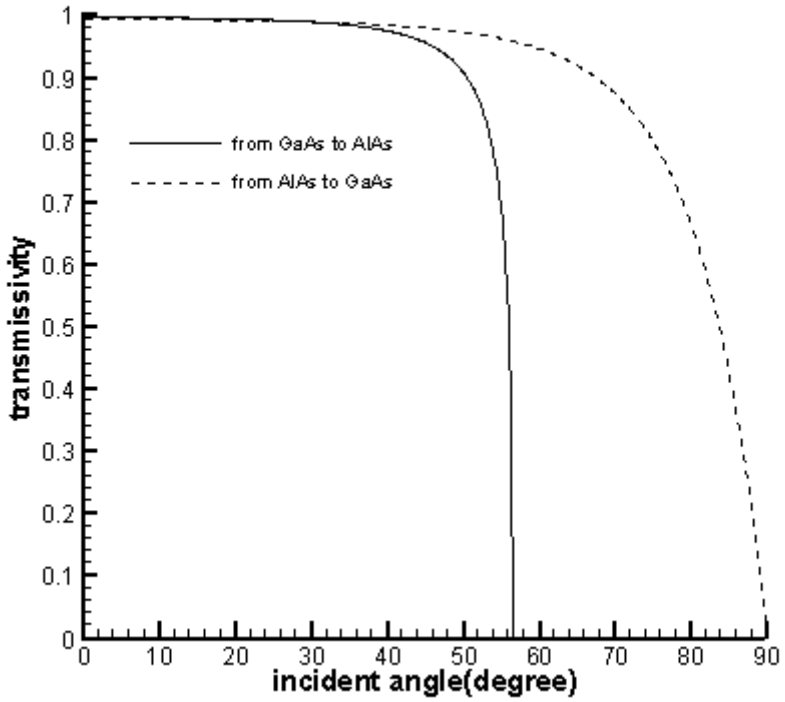

Fig. 4.4 The relation of transmissivity coefficient and incident angles for AMM

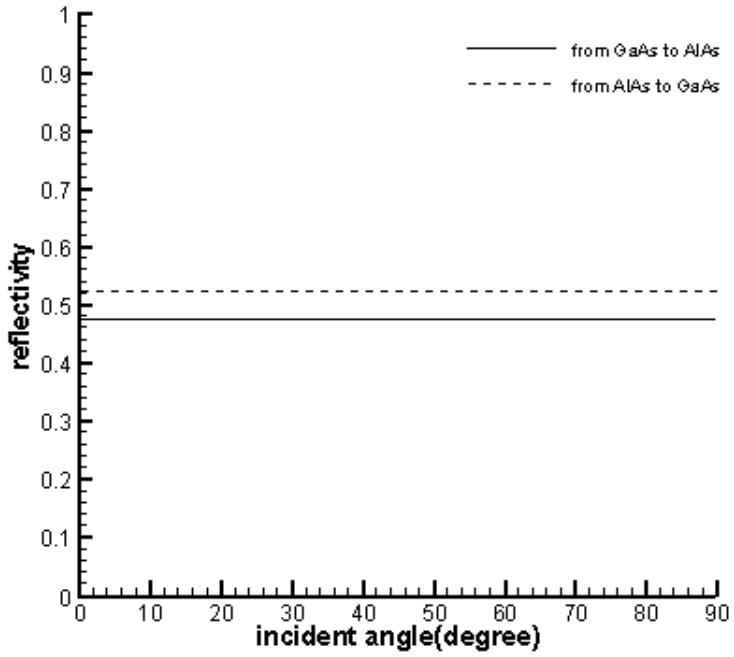

Fig. 4.5 The relation of reflection coefficient and incident angles for DMM

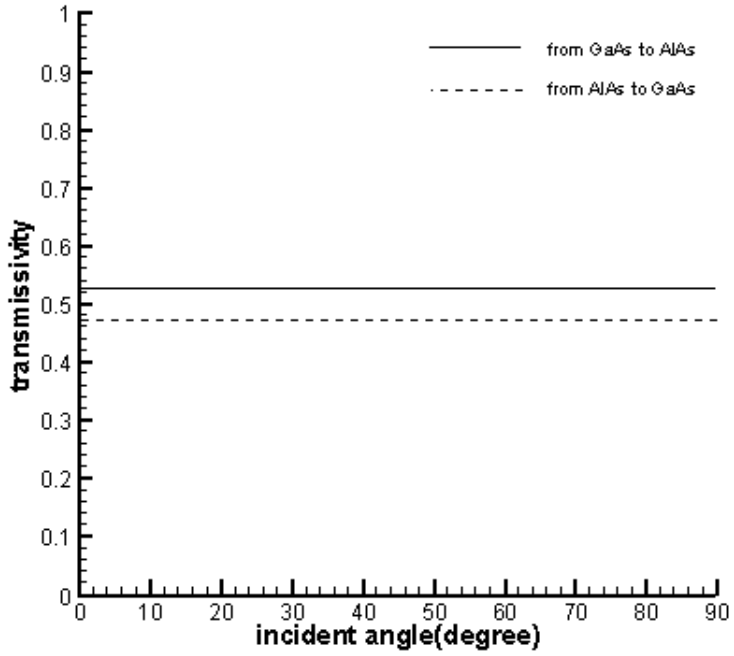

Fig. 4.6 The relation of transmissivity coefficient and incident angles for DMM

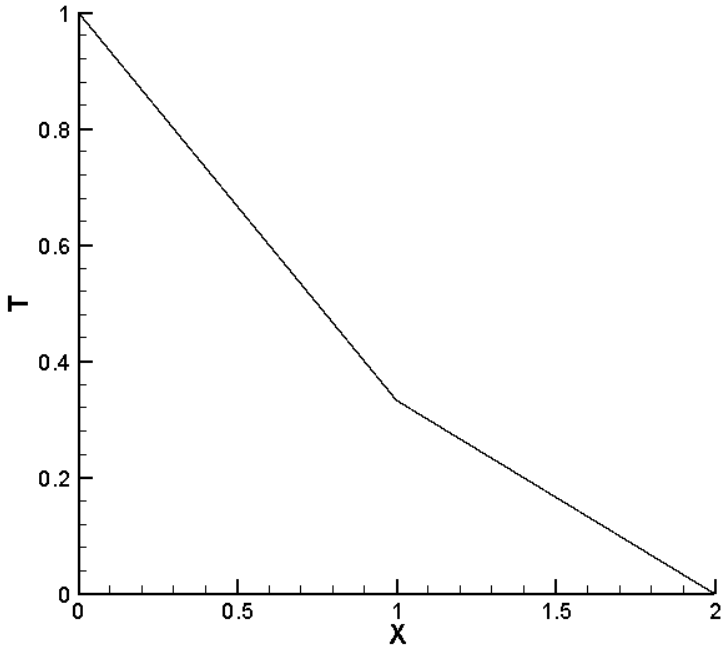

(a)

Fig. 4.7 The temperature distribution for Fourier's law approach on GaAs/AlAs

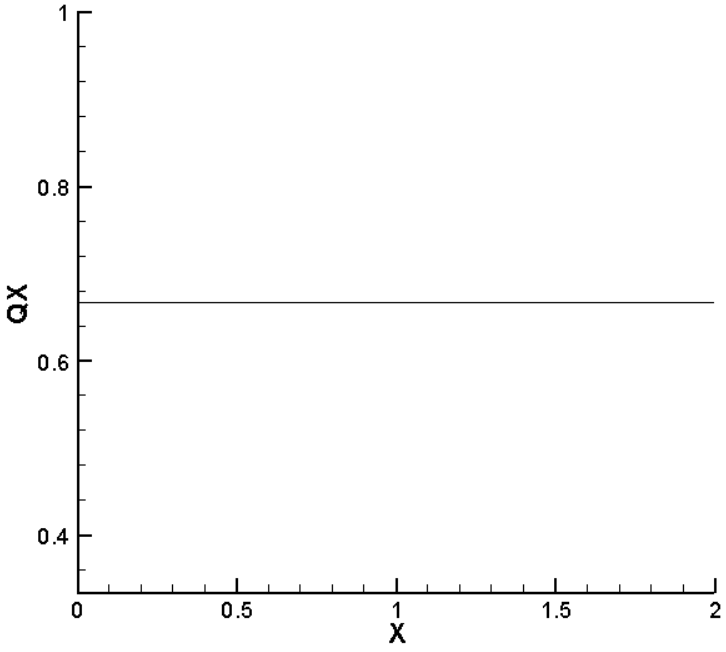

(b)

Fig. 4.8 The heat flux distribution for Fourier's law approach on GaAs/AlAs

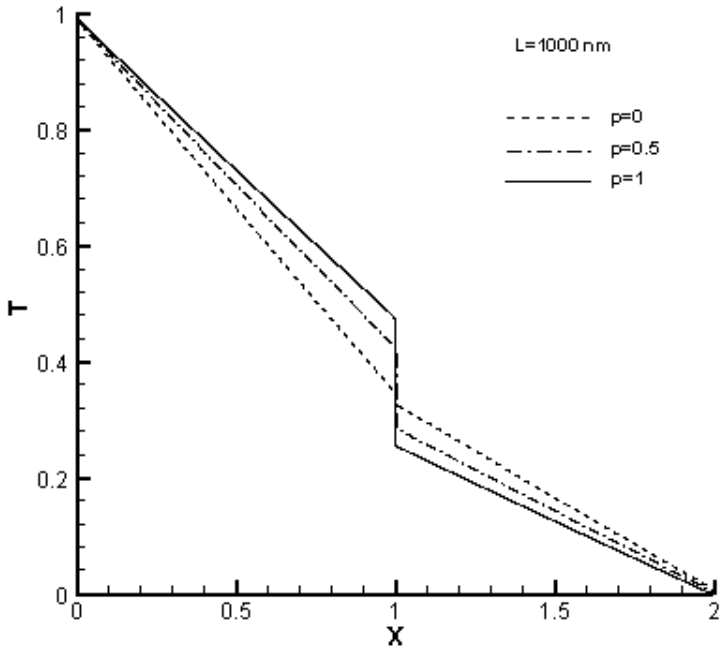

Fig. 4.9 The temperature distributions for L=1000nm on GaAs/AlAs with AMM and DMM interfaces.

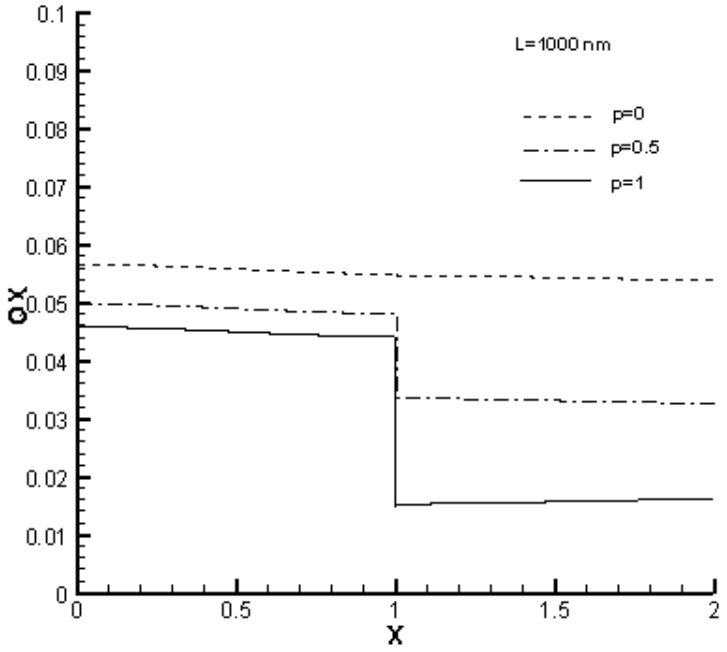

Fig. 4.10 The heat flux distribution for L=1000nm on GaAs/AlAs with AMM and DMM interfaces.

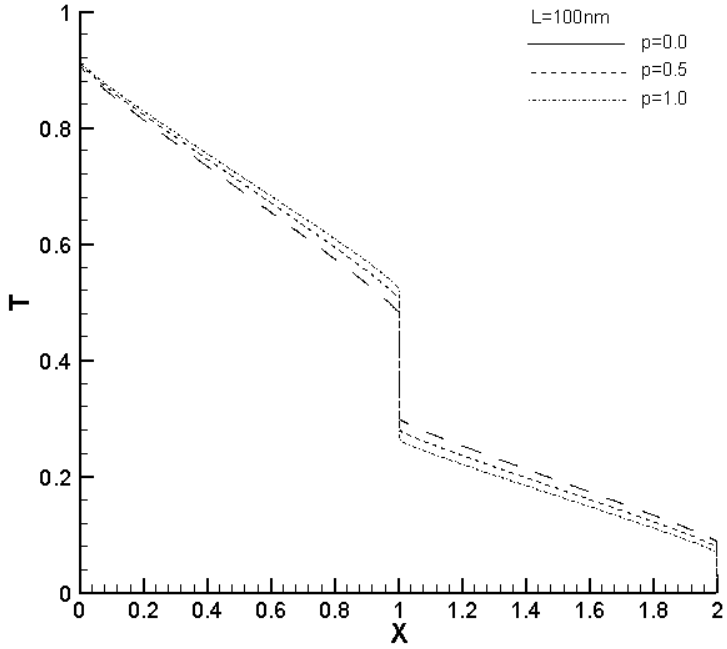

Fig.4.11 The temperature distribution for L=100nm on GaAs/AlAs with AMM and DMM interface

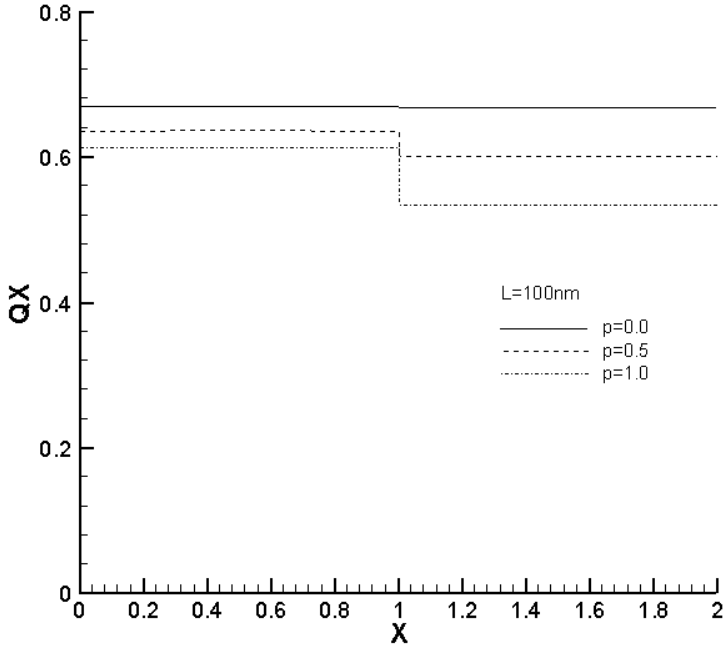

Fig. 4.12 The temperature and heat flux distributions for L=100nm on GaAs/AlAs with AMM and DMM interfaces.

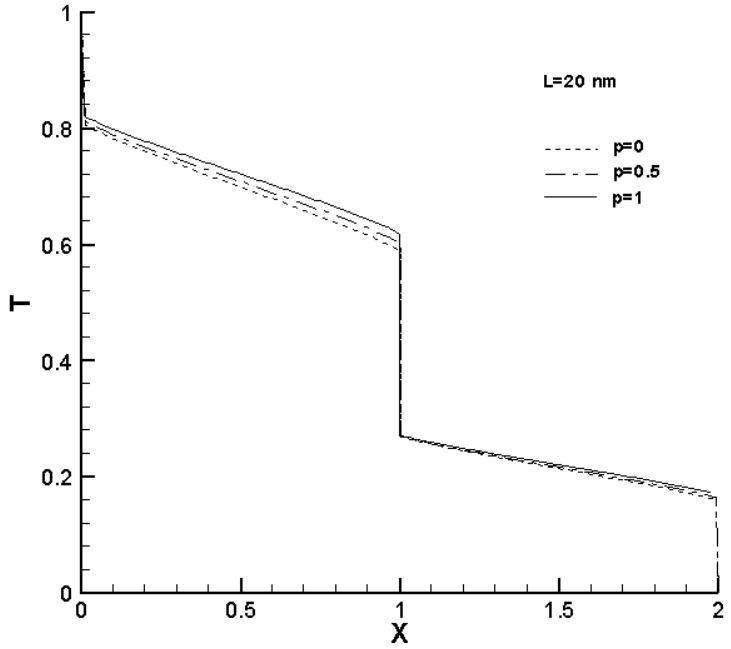

Fig. 4.13 The temperature distribution at steady state for L=20nm on GaAs/AlAs with AMM and DMM interfaces.

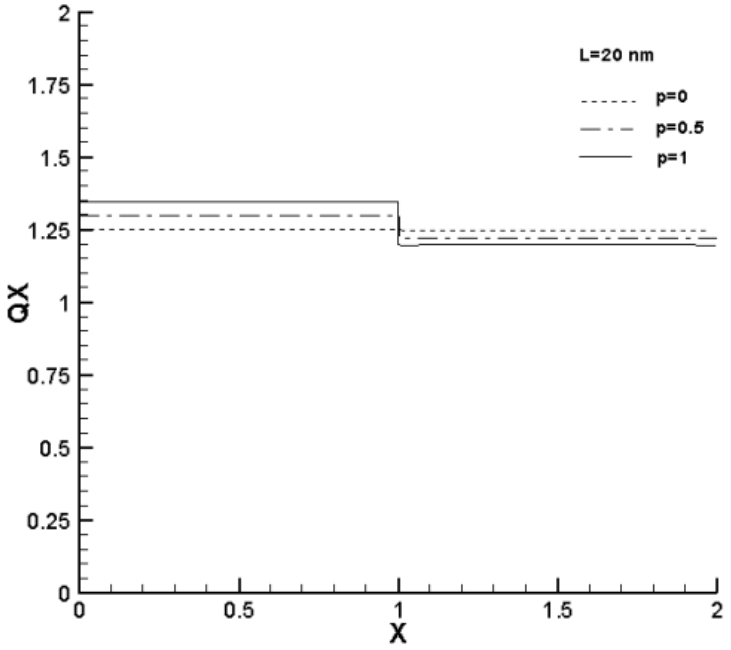

Fig. 4.14 The heat flux distribution at steady state for L=20nm on GaAs/AlAs with AMM and DMM interfaces.

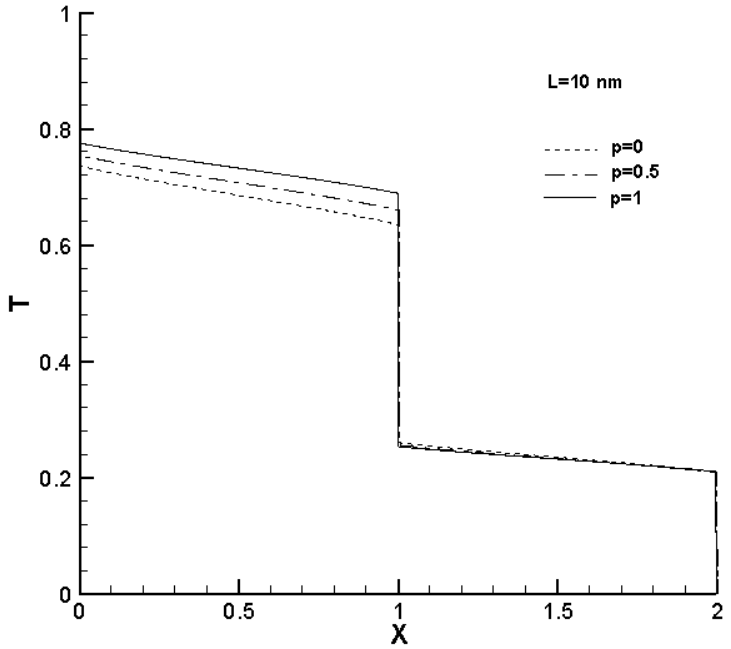

Fig. 4.15 The temperature distribution at steady state for L=10nm on GaAs/AlAs with AMM and DMM interfaces.

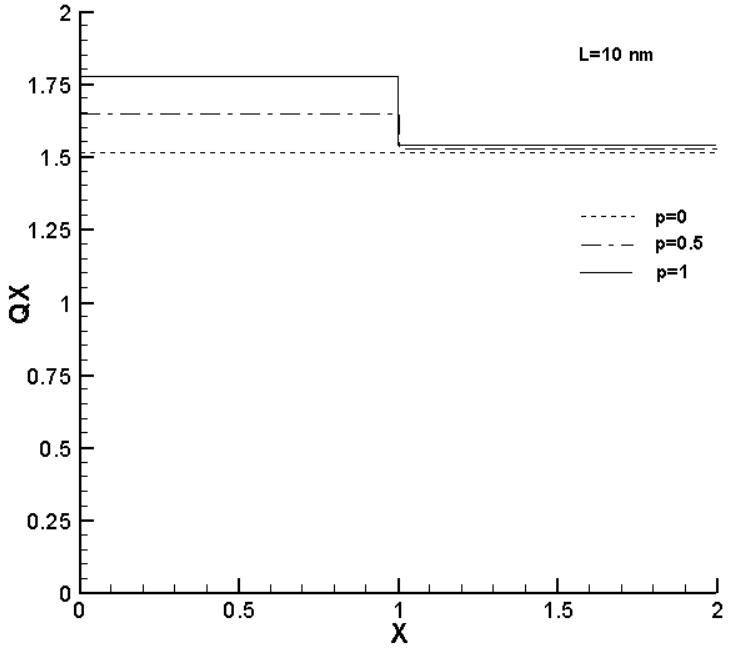

(b)

Fig. 4.16 The heat flux distribution at steady state for L=10nm on GaAs/AlAs with AMM and DMM interfaces.

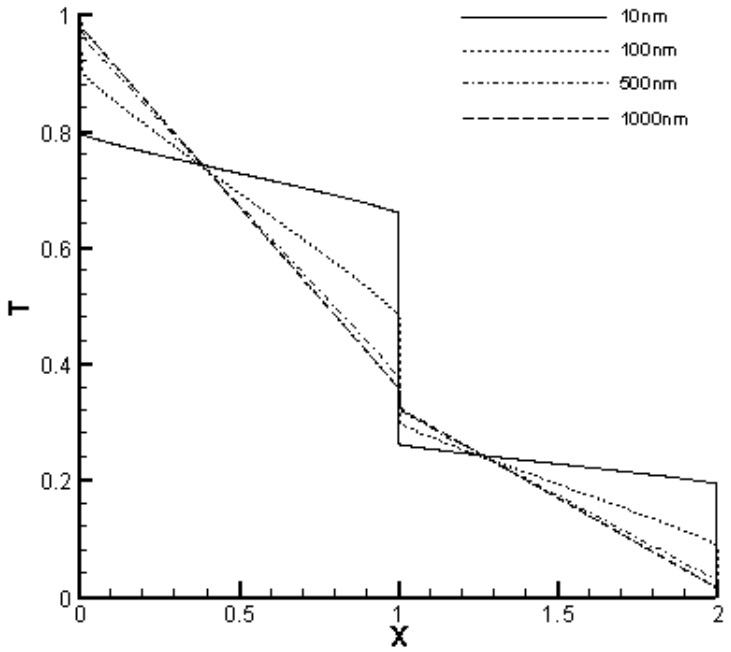

Fig. 4.17 The temperature distribution for different thickness with DMM interface.

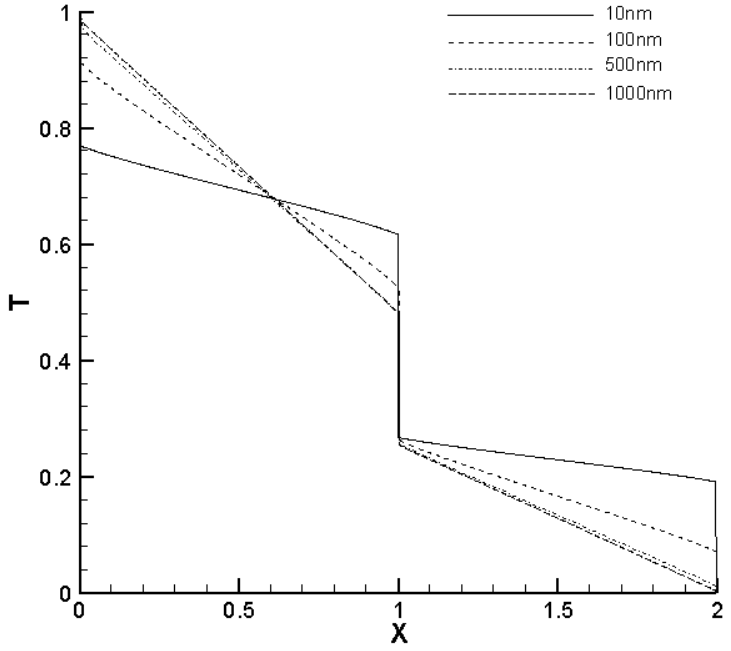

Fig. 4.18 The temperature distribution for different thickness with AMM interface.

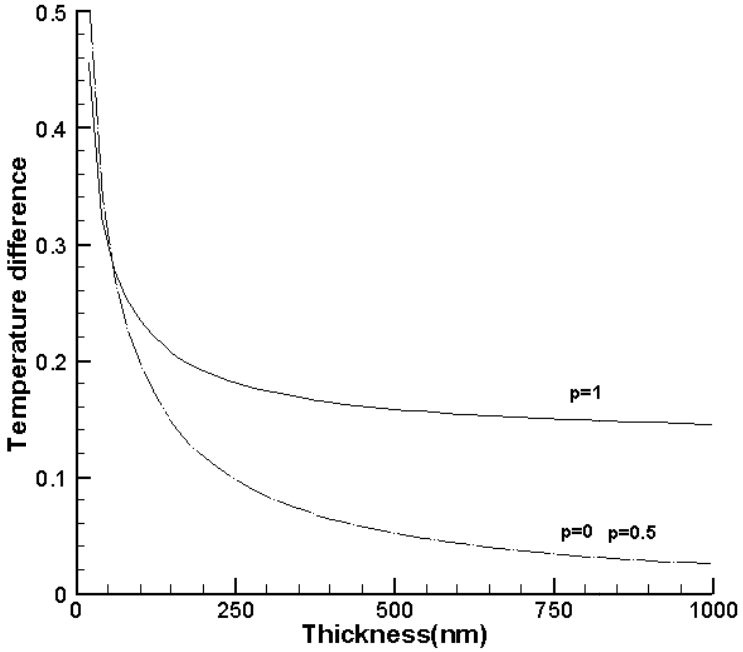

Fig.4.19 The temperature jumps at interface for diffuse and specular interfaces

Fig. 4.20 The thermal conductivity as a function of thickness.

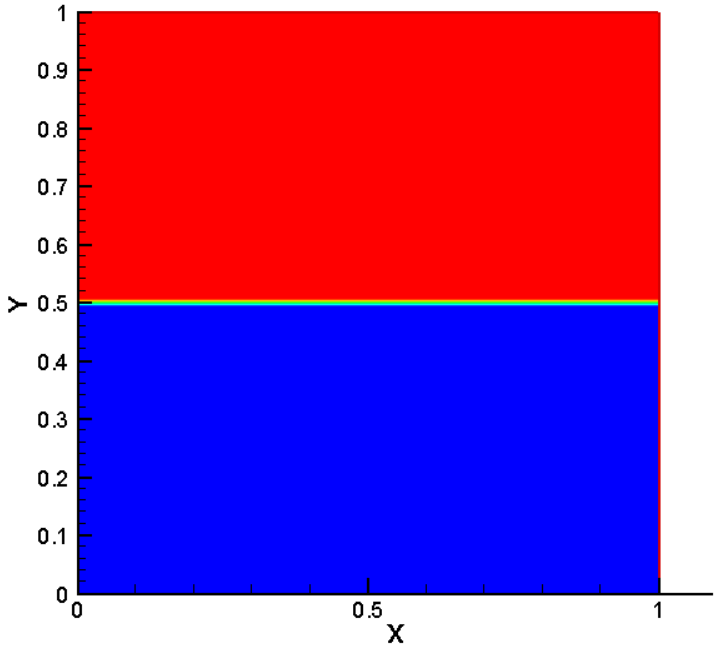

Fig. 4.21 The 2-dimensional inplane sample with one interface Lx=100nm, Ly=100nm. The red is GaAs, and the blue is AlAs.

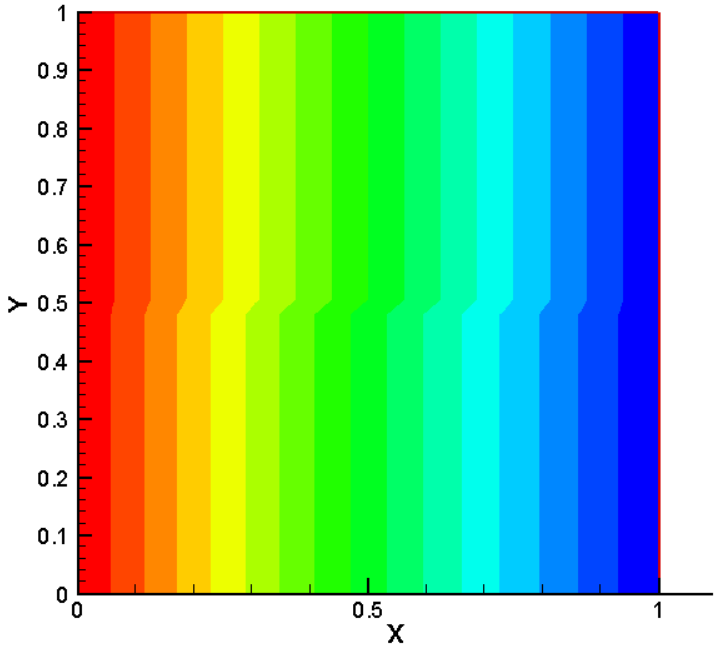

Fig. 4.22 The temperature distribution for one-interface sample.

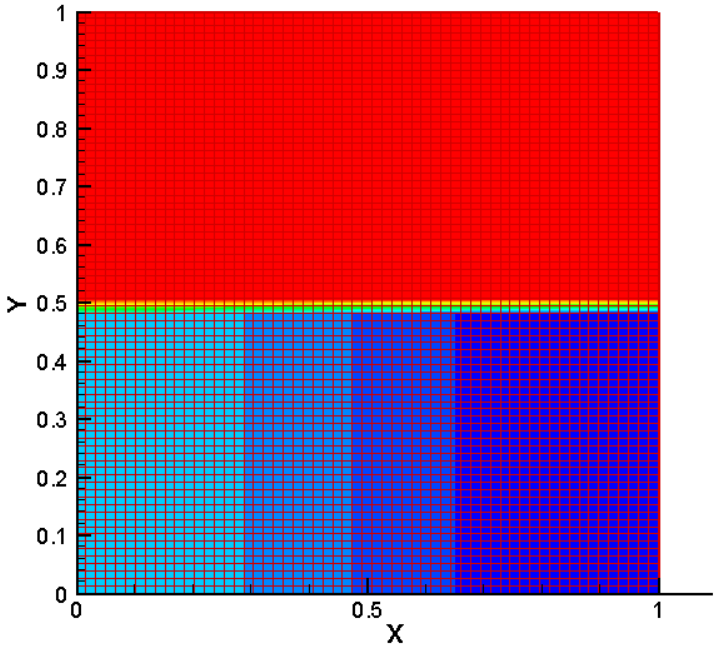

Fig. 4.23 The heat flux distribution in x-direction for one-interface sample (a).

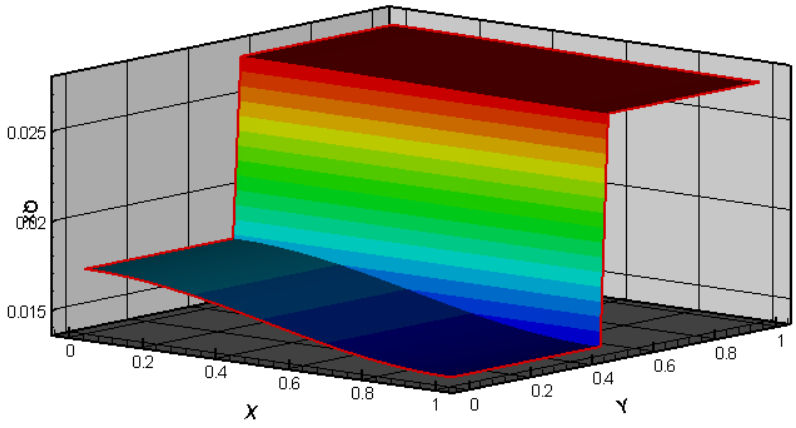

Fig. 4.24 The heat flux distribution in x-direction for one-interface sampleb (b) .

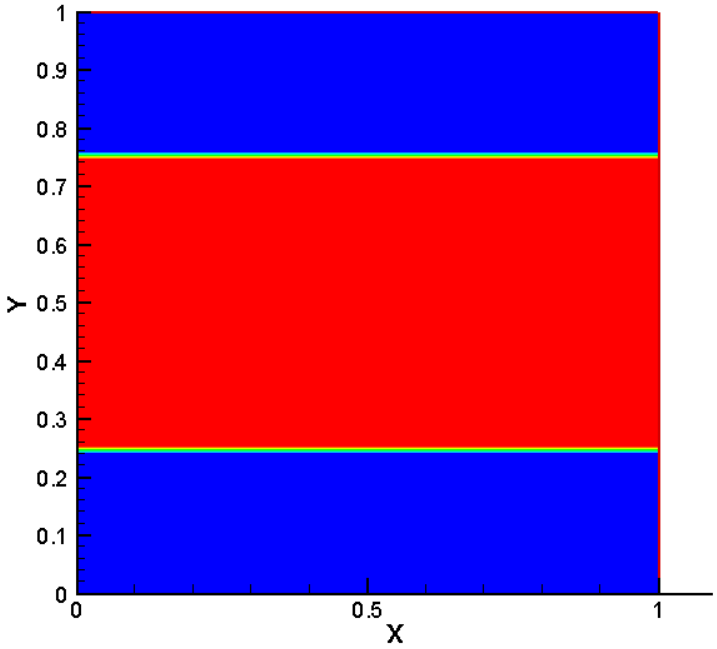

Fig. 4.25 The 2-dimensional inplane sample with two interfaces. Lx=100nm,Ly=100nm. The red is GaAs, and the blue is AlAs

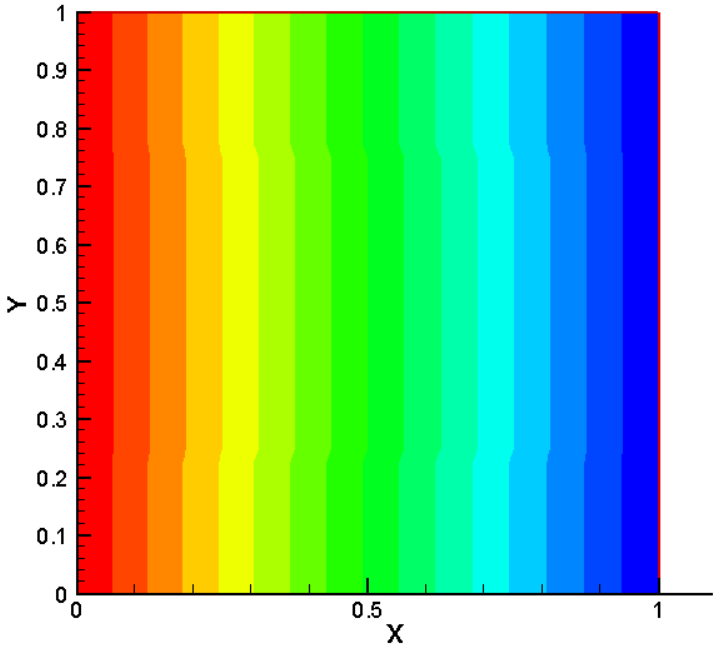

Fig. 4.26 The temperature distribution for the two-interface sample

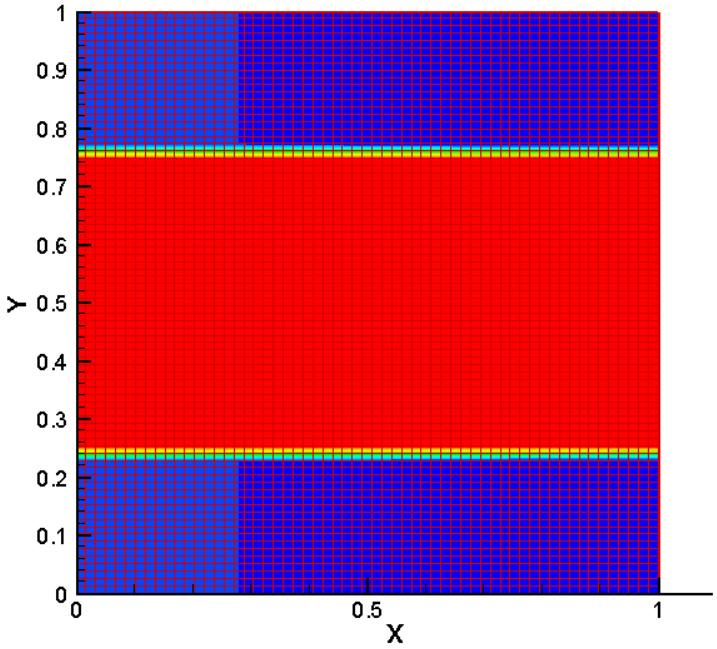

Fig.4.27 The heat flux distribution in x-direction for the two-interface sample (a).

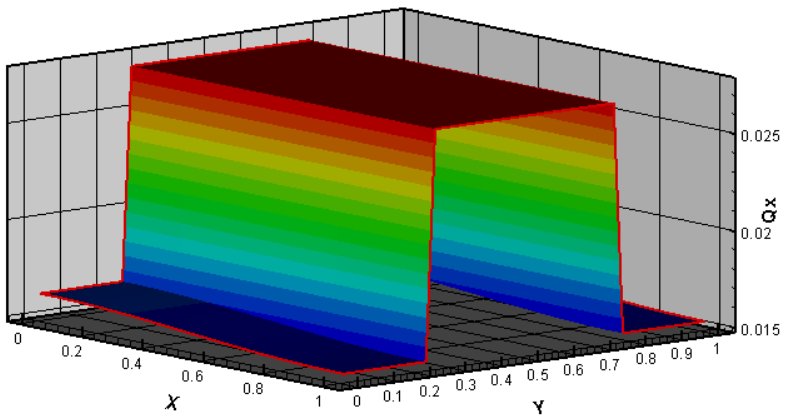

Fig.4.28 The 3-D heat flux distribution in x-direction for the two-interface sample (b).

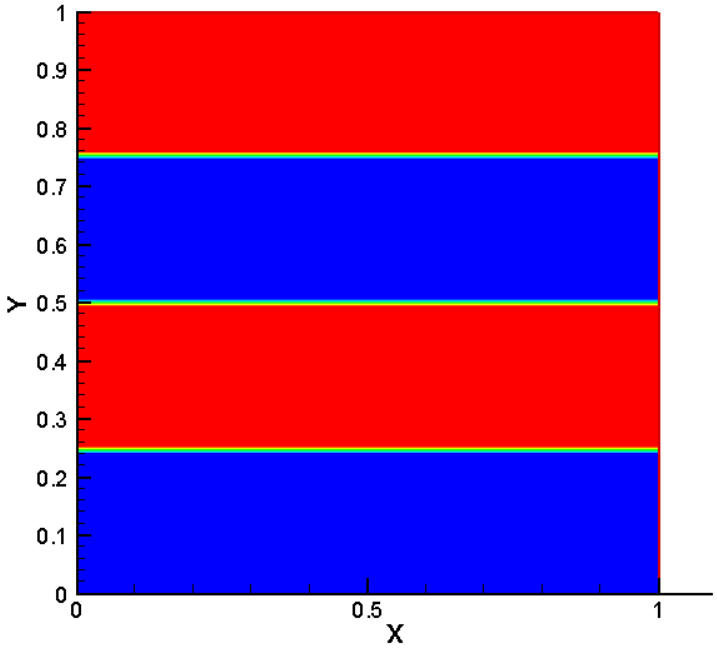

Fig.4.29 The 2-dimensional inplane sample with three interfaces.Lx=100nm,Ly=100nm. The red is GaAs, and the blue is AlAs.

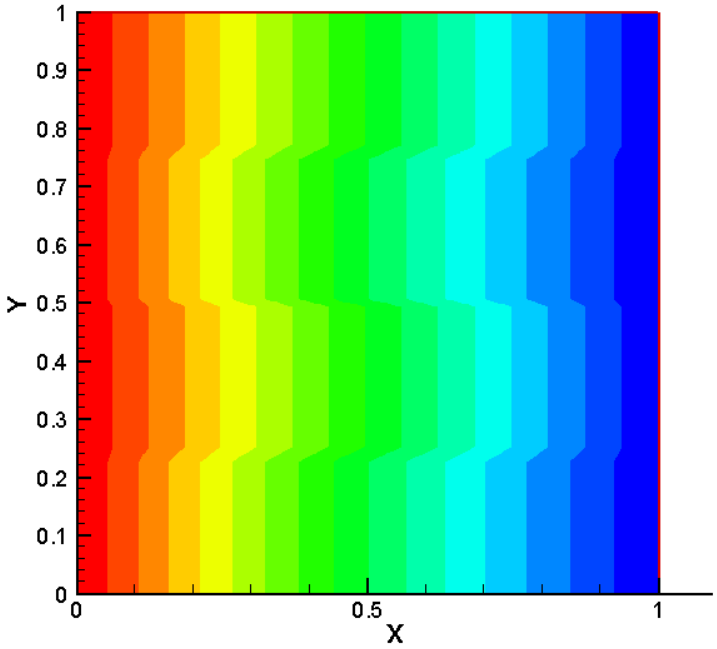

Fig. 4.30 The temperature distribution for the three-interface sample.

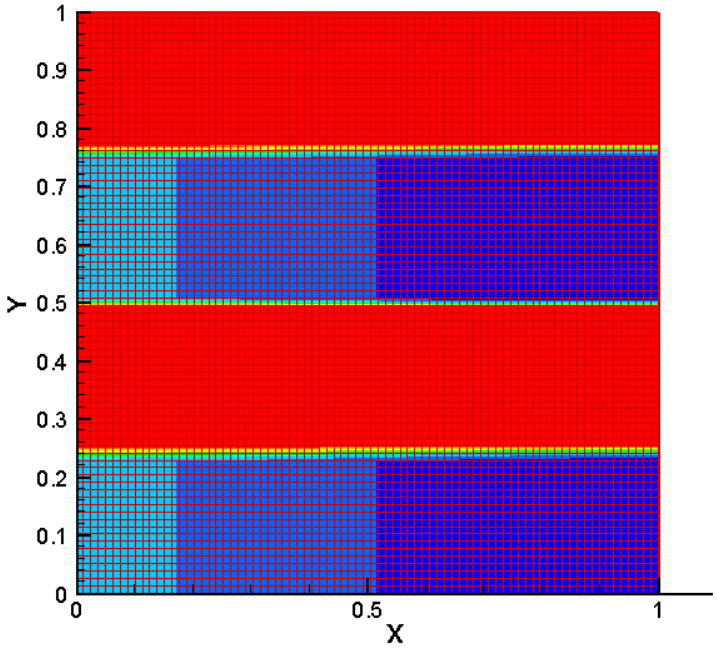

Fig. 4.31 The heat flux distribution in x-direction for the three-interface sample(a).

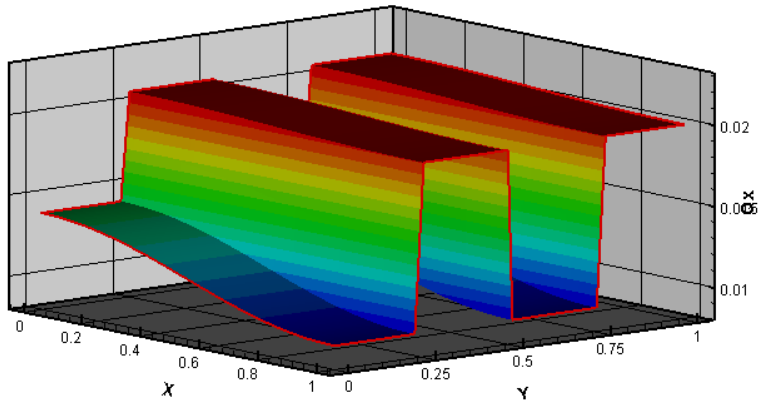

Fig. 4.32 The 3-D heat flux distribution in x-direction for the three-interface sample.

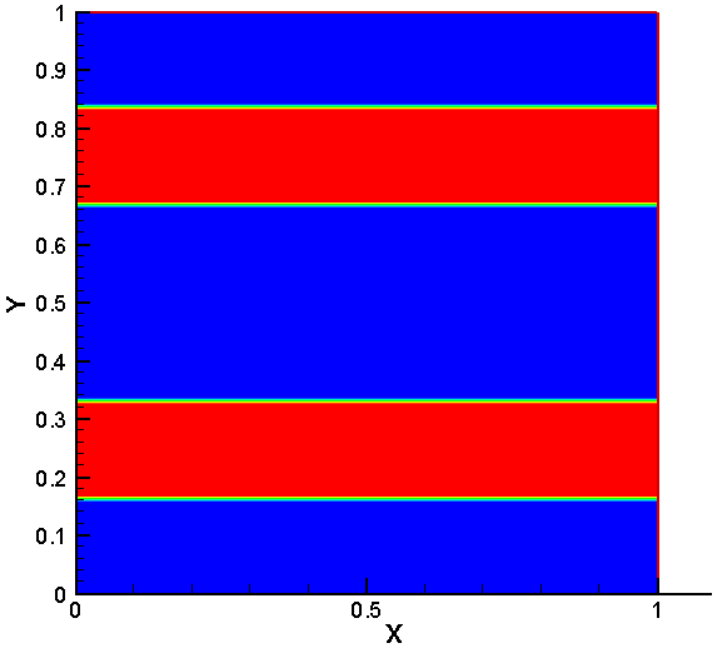

Fig. 4.33 The 2-dimensional inplane sample with four interfaces.Lx=100nm,Ly=100nm. The red is GaAs, and the blue is AlAs.

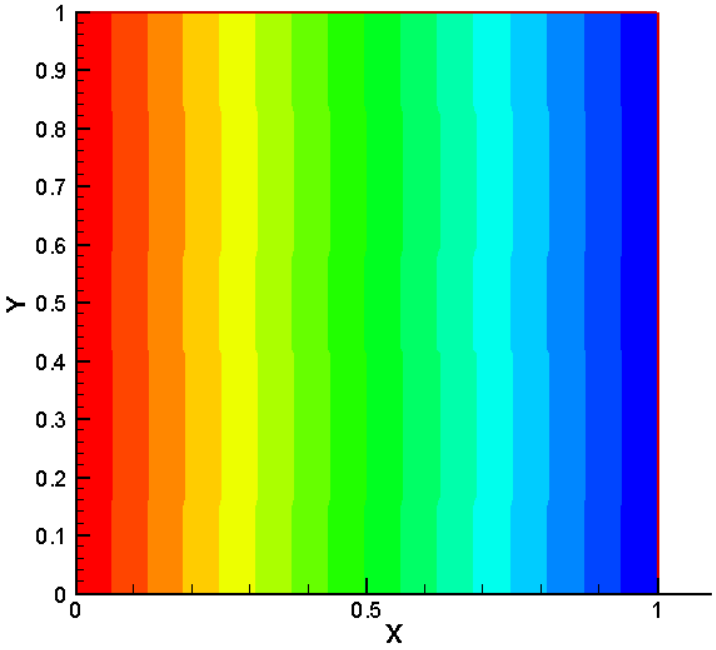

Fig. 4.34 The temperature distribution for the four-interface sample.

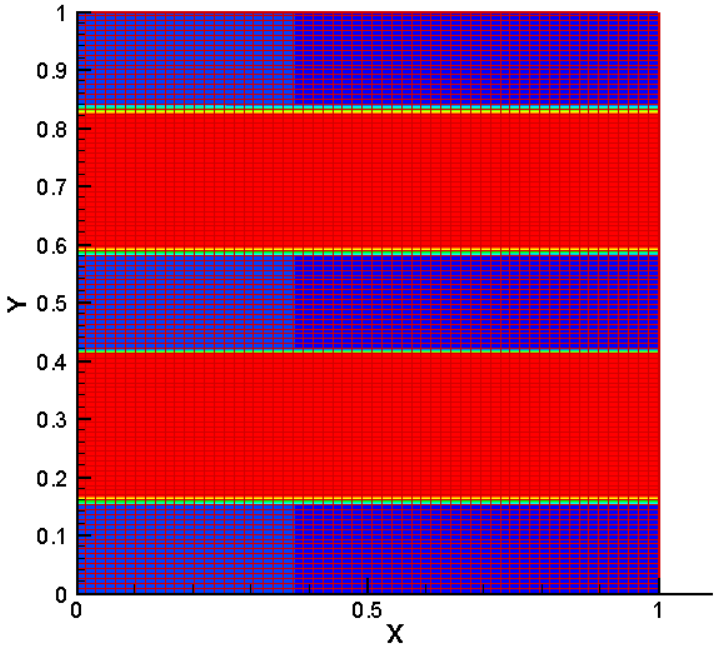

Fig.4.35 The heat flux distribution in x-direction for the four-interface sample.

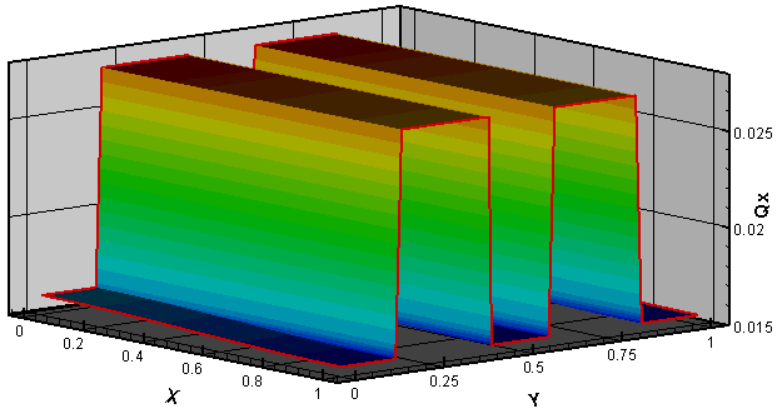

Fig.4.36 The 3-D heat flux distribution in x-direction for the four-interface sample.

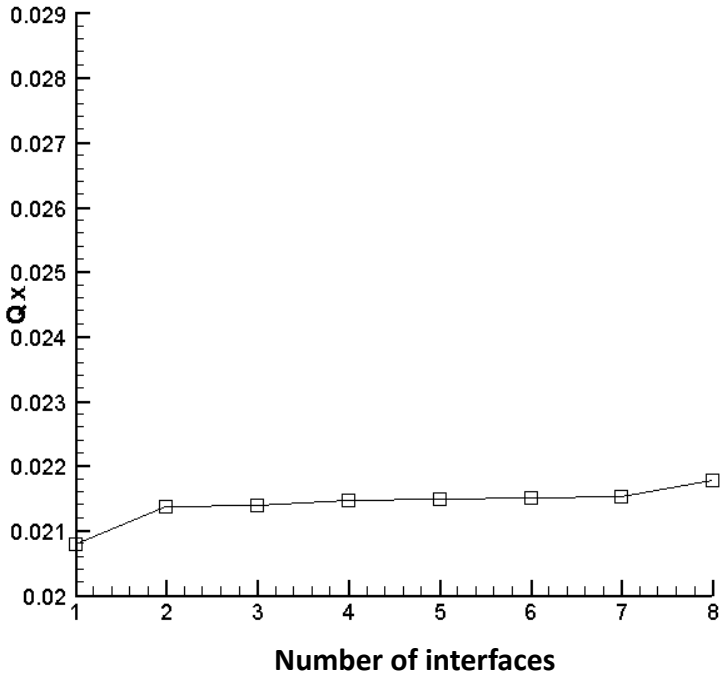

Fig. 4.37 The relation of heat flux in x-direction and their corresponding number of interfaces

Reference

1. Chen, G. , “Thermal Conductivity and Ballistic-Phonon Transport in the Cross-Plane Direction of Superlattices,” Physical Reviews B, Vol.57, pp.14958-14973, 1998.
2. Chen, G., Nanascale Energy Transport and Conversion, Oxford Univeristy Press, 2005.
3. Chen. G., “Size and Interface Effects on Thermal Condutivity of Superlattices and Periodic Thin-Film Structures,” ASME Journal of Heat Transfer, Vol.69, pp.220-229, 1997.
4. Kittel, C., Introduction to Solid State Physics, John Wiley & Sons, 8th Edition, 2004.
5. Majumdar, A., “Microscale Heat Conduction in Dielectric Thin Films,” Journal o of Heat Transfer, Vol. 115, Feb. 1993.
6. Little, W. A., “The Transport of Heat Between Dissimilar Solids at Low Temperature,” Canadian Journal of Physics, Vol.37, pp. 334-349, 1959.
7. LeVeque, R. J., Numerial Methods for Conservation Laws, Oscar E. Lanford, USA, 1992.
8. Modest, M. F., Radiative Heat Transfer, McGraw-Hill, Inc, 1993.
9. Phelan, P. E., “Application of Diffuse Mismatch Theory to the Prediction of Thermal Boundary Resistance in Thin-Film High-Tc Superconductions,” ASME Journal of Heat Transfer, Vol.120, pp. 37-43, 1998.
10. Prasher, R. S. and Phelan, P. E., “A Scattering-Mediated Acoustic Mismatch Model for The Prediction of Thermal Boundary Resistance,” ASME Journal of Heat Transfer, Vol., pp.105-112, 2001.
11. Swartz, E. T. and Pohl, R. O., “Thermal Boundary Resistance,”Reviews of Modern Physics, Vol. 61, pp. 605-668, 1989.

12. Ziman, J. M., Electrons and Phonons, Oxford University Press, London.
13. 謝澤揚, “聲子熱傳輸與理想量子氣體動力學之高解析算則,” 國立台灣大學應用力學研究所博士論文,” 台北, 2007.
14. 林義傑, “應用高解析算則及修正分離座標法之微觀薄膜熱傳分析,” 國立台灣大學應用力學研究所碩士論文,” 台北, 2007.